

**UCGE Reports  
Number 20054**

Department of Geomatics Engineering

**An Analysis of Some Critical Error Sources  
in Static GPS Surveying**

(URL: <http://www.geomatics.ucalgary.ca/links/GradTheses.html>)

by

**Weigen Qiu**

**December 1993**



THE UNIVERSITY OF CALGARY

**An Analysis of Some Critical Error Sources  
in Static GPS Surveying**

by

Weigen Qiu

A THESIS

SUBMITTED TO THE FACULTY OF GRADUATE STUDIES  
IN PARTIAL FULFILLMENT OF THE REQUIREMENTS FOR THE  
DEGREE OF MASTER OF SCIENCE

DEPARTMENT OF GEOMATICS ENGINEERING

CALGARY, ALBERTA

DECEMBER, 1993

© Weigen Qiu 1993

## ABSTRACT

Some critical error sources in static GPS surveying and methods to reduce these errors on baseline determinations are investigated. Ambiguity search strategies in rapid static surveying are discussed and some modifications are explored. Based on the assumption that the impact of the periodic multipath error on code and carrier phase measurements can be minimized by averaging the observations, an attempt is made to estimate the site occupation time in order to correctly resolve the integer ambiguities using spectral analysis in post-processing mode. The relationship between code and carrier phase multipath is investigated. For single frequency users, an ionospheric model is developed by using code and carrier phase measurements. The accuracy of this model and results of baselines by applying this model are analysed.

## ACKNOWLEDGEMENTS

I wish to express my sincere appreciation to my supervisor, Professor Gérard Lachapelle, for his continuous support and encouragement through the course of my graduate studies. His advice and guidance were essential for the completion of this thesis.

Special thanks are extended to Professor M. Elizabeth Cannon for the valued time and knowledge she shared in discussing GPS data processing techniques and problems related to my research, and for providing RAPID and SEMIKIN™ software packages. Mr. D.S. Chen, Mr. G. Lu and Mr. C. Liu are all thanked for their assistance in data collection. Special thanks are also extended to Mr. Karl Grebe, whose helpful grammar checking polished the English writing. The many other graduate students and faculty members who have made the course of my graduate studies both fruitful and enjoyable, are sincerely appreciated.

Parts of my studies were financially supported through grants and contracts from the Natural Science and Engineering Research Council and the Geodetic Survey Division, Canada Centre for Surveying, Energy Mines and Resources Canada. Their contribution is gratefully acknowledged.

Finally, thanks go to my wife Hong Cheng for her support, encouragement and patience.

## TABLE OF CONTENTS

APPROVAL PAGE.....	ii
ABSTRACT.....	iii
ACKNOWLEDGEMENTS .....	iv
TABLE OF CONTENTS .....	v
LIST OF TABLES .....	viii
LIST OF FIGURES .....	x
CHAPTER	
1. INTRODUCTION .....	1
1.1 Background and Previous Studies.....	1
1.2 Thesis Objective.....	5
1.3 Thesis Outline.....	5
2. POSITIONING WITH GPS.....	8
2.1 System Description .....	8
2.2 GPS Signals .....	9
2.3 GPS Observations.....	11
2.4 Major Error Sources in GPS Observations.....	12
2.4.1 Orbital Errors.....	13
2.4.2 Clock Errors.....	14
2.4.3 Ionospheric Delay .....	15
2.4.4 Tropospheric Delay.....	16
2.4.5 Multipath.....	16

2.4.6 Receiver Noise.....	17
3. RAPID STATIC DGPS.....	19
3.1 Carrier Phase Ambiguity Resolution in Rapid Static DGPS .....	20
3.1.1 Carrier Phase Ambiguity Float Solution.....	22
3.1.2 Ambiguity Searching Window .....	23
3.1.3 Testing of Integer Ambiguity Combinations.....	24
3.1.4 Assurance of the Integer Ambiguity .....	27
3.1.5 A Fast Quadratic Form Testing Algorithm.....	28
3.2 The Influence of Satellite Geometry on Ambiguity Resolution .....	31
3.2.1 Ambiguity Resolution Prediction Algorithm.....	32
3.2.2 Numerical Results.....	35
4. MULTIPATH EFFECT ON RAPID STATIC DGPS.....	41
4.1 Code and Carrier Multipath.....	43
4.2 Multipath Detection and Reduction.....	48
4.2.1 Code Multipath Detection .....	48
4.2.2 Carrier Phase Multipath Detection.....	51
4.2.3 Multipath Error Reduction .....	56
4.3 Multipath Effect on Rapid Static DGPS.....	59
5. IONOSPHERIC EFFECT MODELING FOR SINGLE FREQUENCY USERS .....	63
5.1 The Ionosphere and GPS Signal Propagation.....	64
5.2 Ionospheric Effect on Baseline Determination.....	68
5.3 Ionospheric Effect Modeling for Single Frequency Users .....	72
5.3.1 Ionospheric Effect Modeling Using Code and Phase	

Measurements.....	72
5.3.2 Separation of Carrier Phase Ambiguity and Ionospheric Delay .....	74
5.3.3 Results and Analysis.....	76
5.3.4 Recovery of the Ionospheric Delay with the Divergence Method for Baseline Determination .....	85
6. CONCLUSIONS AND RECOMMENDATIONS.....	90
REFERENCES.....	94

## LIST OF TABLES

### Table

2.1	Relative Accuracy and Orbital Errors .....	13
2.2	Tropospheric Delay on Measured Ranges.....	16
2.3	Receiver Noise for Different Observations.....	18
3.1	Satellite Elevation Angles for 442 m Baseline Data.....	35
3.2	Rapid Static Test Results for 442 m Baseline.....	37
3.3	Satellite Elevation Angles for 519 m Baseline Data.....	38
3.4	Rapid Static Test Results for 519 m Baseline.....	39
4.1	Multipath Analysis of Ashtech P-XII for Satellite 11 .....	58
4.2	Major Multipath Periods in 519 m Baseline.....	61
4.3	Success Rate of Trials Using Different Observation Time.....	61
5.1	Maximum Vertical Ionospheric Range Error.....	67
5.2	Ionospheric Effect on Baseline Solution.....	69
5.3	Rapid Static Tests with and without Dual Frequency Ionospheric Corrections Applied.....	71
5.4	Relative Errors of the Ionospheric Delay Estimated with a L1 Narrow Correlator Spacing Receiver.....	82
5.5	Comparison of L1, L1/L2 and Code/Carrier Divergence Solutions (Baseline ALBH-DRAO, 301.77km) .....	87
5.6	Comparison of L1, L1/L2 and Code/Carrier Divergence Solutions (Baseline ALBH-HOLB, 419.24km).....	87

5.7	Comparison of L1, L1/L2 and Code/Carrier Divergence Solutions (Baseline DRAO-DRAO, 627.13km).....	88
5.8	RMS Fit of L1, L1/L2 and Code/Carrier Divergence Solutions .....	88

## LIST OF FIGURES

### Figures

2.1	Frequency and Signal Generation of GPS Satellites.....	10
3.1	General Strategy of Rapid Static Ambiguity Resolution.....	21
3.2	Evolution of Formal Phase Ambiguity Precision for 442 m Baseline (L1).....	36
3.3	Evolution of Formal Phase Ambiguity Precision for 519 m Baseline (L1) .....	38
3.4	Double Difference Residuals of Satellite Pair SV17-SV23 for 519 m Baseline .....	39
4.1	Multipath Caused by Reflection .....	41
4.2	Noncoherent DLL Structure.....	44
4.3	Multipath Effect on Carrier Phase.....	46
4.4	Code Multipath Error on Day 342.....	49
4.5	Code Multipath Error on Day 343.....	50
4.6	Cross-Correlation Function of Multipath.....	51
4.7	Differential Ionospheric Delay for SV03 on Day 314.....	54
4.8	Differential Ionospheric Delay for SV03 on Day 315.....	55
4.9	Correlation of Differential Ionospheric Delays between Day 314 and Day 315 .....	55
4.10	Accuracies of Float Ambiguity Estimation.....	61
4.11	Code and Carrier Multipath.....	62

5.1	Approximate Positions of Ottawa GPS Network Stations.....	69
5.2(a)	Comparison of Ionospheric Delay Estimated by The Dual-frequency and P(L1) Code-Carrier Divergence Method (SV23, and 17) .....	78
5.2(b)	Comparison of Ionospheric Delay Estimated by The Dual-frequency and P(L1) Code-Carrier Divergence Method (SV20, 21 and 26) .....	79
5.3(a)	Comparison of Ionospheric Delay Estimated by The Dual-frequency and C/A(L1) Code-Carrier Divergence Method (SV03 and 17).....	81
5.3(b)	Comparison of Ionospheric Delay Estimated by The Dual-frequency and C/A(L1) Code-Carrier Divergence Method (SV21 and 26).....	81
5.4	Local Irregularities of Code-Carrier Phase Divergence Measurements .....	82
5.5	Polar Plots of Satellites, 10:00-13:00, December 8, 1992.....	84
5.6	Broadcast Ionospheric Delay Versus Delay Estimated Using Code/Carrier Divergence (SV23) .....	84
5.7	Broadcast Ionospheric Delay Versus Delay Estimated Using Code/Carrier Divergence (SV03 and 26) .....	84
5.8	ACS Stations Used for Baseline Test .....	86

## CHAPTER 1

### INTRODUCTION

#### 1.1 BACKGROUND AND PREVIOUS STUDIES

The NAVSTAR GPS (NAVigation System with Time and Ranging Global Positioning System) is a satellite-based radio navigation system providing precise three-dimensional position, navigation, and time information to suitably equipped users. The system will be continuously available on a world-wide basis, and is independent of meteorological conditions [Leick, 1990; Seeber, 1993; and Wells et al., 1987]. The initial intention was to use this system mainly for navigation purposes of the US military. Due to the tremendous accuracy potential of this system, and the latest improvements in receiver technology, there is a growing community which utilizes the GPS for a variety of civilian applications. GPS surveying is only a small part of the total spectrum of the many uses of GPS. The applications of GPS surveying can be divided into three categories:

(1) *Conventional static GPS surveying.* Receivers are kept on individual sites for several hours or even several days. The primary objective of this kind of GPS surveying is accuracy. The required site occupation time and hence the efficiency plays a subordinate role. The main applications of conventional static GPS surveying are to establish local, regional, or even global networks. Static GPS

carrier phase relative positioning has yielded accuracy of a few parts per 100 million [Erickson, 1992; Lichten and Bertiger, 1989].

(2) *Rapid static surveying*. As the name implies, rapid static surveying involves a short static site occupation of only a few minutes. GPS code and phase data is post-processed using a variety of statistical ambiguity search algorithms to provide baseline precision commensurate with static survey methods [Frei, 1991]. Since rapid static surveying dramatically increases GPS surveying efficiency, it will certainly be widely used in future surveying applications, such as cadastral surveying and the establishment of Geographic Information Systems (GIS).

(3) *Kinematic surveying*. This implies the need for ambiguity resolution at the beginning of the session, times of cycle slip occurrences, and rising of new satellites [Abidin, 1993]. Post processing of kinematic GPS data is already very advanced [Abidin, 1990; Cannon et al., 1990; Chen, 1993; Wübbena, 1989]. Kinematic GPS positioning can also be used to achieve accurate, real-time positions and velocities of a moving platform on land, in the air, and at sea.

GPS observations are subject to a number of errors, both random and systemic. The major error sources include receiver noise, orbital and clock errors, and propagation errors (ionospheric effect, tropospheric effect, and multipath). Receiver noise largely depends on the system architecture. Modern receiver technology tends to bring the internal phase noise below 1 mm, and to reduce the code resolution to the decimetre level. Orbital and clock errors can be reduced or eliminated by using *a posteriori* precise ephemerides and forming double difference observations. Various models have been developed to estimate the tropospheric delay. The dry component can be precisely described by these

models with an accuracy of  $\pm 1\%$ , while the wet component can be modeled by surface weather data to within 3-4 cm [Wells et al., 1987]. If the stations are close together, the tropospheric residual error almost completely disappears by differencing in relative mode. For a long baseline, direct measurements with water vapor radiometers may be used [Elgered et al., 1985].

Although various measures can be taken to reduce the multipath error in kinematic and rapid static surveying, multipath error contamination is still inevitable in many cases. For a short baseline, multipath error can dominate the adjusted residuals and thus affect the site occupation time needed to resolve the ambiguities. Ionospheric delay is a major source of concern to GPS users since it can reach extreme values of around 50 metres for satellites directly overhead at times of high solar activity, and up to three times this amount for satellites near the horizon [Wells et al., 1987]. The ionospheric effect can be modeled by observing dual-frequency GPS signals. However, as the type of receiver used by the majority of civilian users becomes the less expensive, single frequency kind, there is not enough information to allow elimination of this delay. For precise positioning applications, some methods of eliminating or reducing the ionospheric effect are highly desirable.

Integer ambiguity resolution techniques in rapid static surveying are closely related to the development of kinematic surveying. During the past few years, several techniques for rapid ambiguity resolution have been developed. These include "Extra-widelaning" [Wübbena, 1989; Abidin and Wells, 1990], "Sequential phase ambiguity resolution" [Talbot, 1991], the "Fast ambiguity resolution approach" [Frei and Beulter, 1990], the "Least-squares ambiguity search technique" [Hatch, 1991a; Lachapelle et al., 1992], the "Ambiguity function

method" [Counselman and Gourevitch, 1981; Remondi, 1984], and the "Fast Ambiguity Search Filter (FASF)" [Chen, 1993]. Although each of these techniques has some unique characteristics, each also has elements shared with other ambiguity resolution techniques.

Multipath effects on pseudorange measurements have been studied for almost two decades. In 1973, Hagerman derived relationships involving multipath and code-tracking error [Hagerman, 1973]. This fundamental work formed the basis for the analysis of GPS code and carrier multipath. Lachapelle et al. [1989] described marine DGPS experiments in which multipath was mitigated through the use of RF absorbing ground planes and filtering schemes. Evans [1986] demonstrated multipath effects on ionospherically corrected code and carrier phase measurements from geodetic receivers. Georgiadou and Kleusberg [1988a] considered multiple reflections and showed that multipath on short baselines could be detected using dual frequency measurements. Abidin [1990] examined the effects of multipath on ambiguity resolution for dual frequency measurements. The effect of multipath on ionospheric measurements using GPS was presented by Bishop et al. [1985]. Some receivers have incorporated special features to reduce multipath, like narrow early-late spacing [Van Dierendonck et al., 1992]. Van Nee [1992] studied the tracking performance of the delay lock loop (DLL) and proposed an optimum GPS receiver structure in the presence of multipath.

In spite of the highly variable and irregular character of the ionosphere, various attempts have been made to develop suitable models to describe at least its mean behavior with a reasonable level of accuracy. The International Reference Ionosphere (IRI) can predict the Total Electron Content (TEC) with an

accuracy level of about 30% [McNamara and Wilkinson, 1983]. The model presently offered by the GPS system to single frequency users has been developed by Klobuchar [1987]. It provides a correction for approximately 50% RMS of the ionospheric range error. Georgiadou and Kleusberg [1988b] used a model of ionospheric vertical delays derived from one dual-frequency receiver in the vicinity of a small network to remove the systematic effect of the ionospheric delay. Cohen et al. [1992] and Xia [1992] presented a procedure to estimate the absolute ionospheric delay using single-frequency code and phase measurements. Experimental results show that developments in this field are promising.

## **1.2 THESIS OBJECTIVE**

The objective of this thesis is to investigate the impacts of some critical error sources on static surveying, and explore methods to reduce these errors on baseline determinations. Ambiguity search strategies in rapid static surveying are discussed and some modifications are explored. Based on the assumption that the impact of the periodic multipath error on code and carrier phase measurements can be minimized by averaging the observations, an attempt is made to estimate the site occupation time in order to correctly resolve the integer ambiguities. For single frequency users, an ionospheric model is developed by using code and carrier phase measurements. The accuracy of this model and results of baselines by applying this model are analysed.

## **1.3 THESIS OUTLINE**

The thesis consists of six chapters. The contents of these chapters are as follows:

Chapter 2 gives an introduction of GPS, including a description of the three constituent parts, namely, the control segment, the space segment, and the user segment. The signals transmitted by the satellites are also described, as are the various types of observables. An overview of the error sources and their effects on baseline determination is presented.

Chapter 3 describes the ambiguity search algorithms in rapid static surveying. Various criteria are introduced to isolate the correct integer ambiguities. A fast algorithm to calculate the quadratic form of the adjusted residuals is also presented in this chapter. An algorithm which can be used in real-time to estimate the occupation time needed to resolve the ambiguities in rapid static surveys is described. Finally, numerical results of this algorithm are given.

Chapter 4 investigates multipath effects on rapid static surveys. Multipath errors on pseudorange and carrier phase measurements are discussed. Methods of detecting and reducing multipath errors are presented along with numerical examples. The method of estimating site occupation time in rapid static surveys using spectral analysis of major multipath periods is described.

Chapter 5 investigates the impact of the ionospheric delay on baseline determination. An introduction to ionosphere and radio signal propagation is given. Two examples of the ionospheric effect on baseline determination are presented. One example shows the impact of the dual-frequency ionospheric correction on rapid static surveys for short baselines. Another example shows the errors on baseline components due to the ionospheric effect for baselines of different lengths. The major part of this chapter goes into detail on the

development of ionospheric modeling using code/carrier divergence for single frequency users. Results from various type of receivers are analysed.

Finally, the research is summarized and some conclusions from the results are drawn in Chapter 6. Several recommendations are also made for further investigations.

## CHAPTER 2

### POSITIONING WITH GPS

In this chapter, the Global Positioning System is introduced. As there are a number of introductory references available [Leick, 1990; Wells et al, 1987], a very brief discussion of the basics of the system will be given and only the parts which are relevant to observation modeling and error sources will be discussed in more detail.

#### 2.1 SYSTEM DESCRIPTION

The NAVSTAR Global Positioning System is an all-weather, space-based navigation system under development by the Department of Defense (DoD) of the US to satisfy the requirements for the military forces to accurately determine their position, velocity, and time in a common reference system, anywhere on or near the Earth on a continuous basis [Wooden, 1985]. Due to the tremendous accuracy potential of this system and the latest improvements in receiver technology, there is a growing community which utilizes the GPS for a variety of civilian applications.

The system can be conveniently divided into three units: (1) the space segment, (2) the control segment, and (3) the user segment.

**The Space Segment** is composed of the satellites in orbit. These satellites essentially act as beacons sending signals in a one-way ranging mode with which

users can determine their position, velocity, etc. In addition to sending signals, the satellites can perform several other functions as on-board processing of data, maintenance of very precise time, and maneuvering on demand from the ground control stations [Wells et al., 1987]. After full deployment, the NAVSTAR GPS system will consist of 24 satellites (21+3 active spares) at an altitude of 20,000 km. The satellites are distributed in 6 orbital planes in a manner which ensures the visibility of four or more satellites at all locations on the earth's surface at any time.

**The Control Segment** consists of five ground-based tracking and control stations. The one at Colorado Springs is the Master Control Station (MCS). The coordinates of each tracking station are very precisely known and dual-frequency receivers connected to atomic clocks are used to track the signals from the satellites. The data are then send to the MCS where they are processed to calculate and predict orbits and satellite clock errors. The MCS, along with several other tracking stations, can also transmit commands for satellite movement and upload new ephemerides and clock correction information.

**The User Segment** is the ultimate segment in the chain of system components. It is the GPS receiver, consisting of an antenna, signal tracking circuitry, user interface, power, and a microprocessor to control the operation of the receiver. There are many receivers now commercially available ranging from low-cost, single-frequency sets to expensive dual-frequency devices.

## **2.2 GPS SIGNALS**

GPS satellites broadcast signals on two L-band carrier frequencies; an L1 frequency of 1575.42 MHz and an L2 frequency of 1227.60 MHz. The

corresponding wavelengths are about 19 cm for L1 and 24 cm for L2. Both carrier frequencies are modulated by so called **Pseudo-Random Noise Codes**. The L1 carrier is modulated by the **Coarse Acquisition Code** referred to as the **C/A code**, whereas both carrier frequencies are modulated by the **Precise Code** referred to as the **P-code**. These two codes form the basis for the **Standard Positioning Service (SPS)** and **Precise Positioning Service (PPS)**. In addition, both signals contain the navigation message which is transmitted at a data rate of 50 bits per second. The navigation message contains information such as ephemerides, satellite clock corrections, satellite status and health information. Figure 2.1 shows a scheme of the frequency and signal generation for a particular satellite.

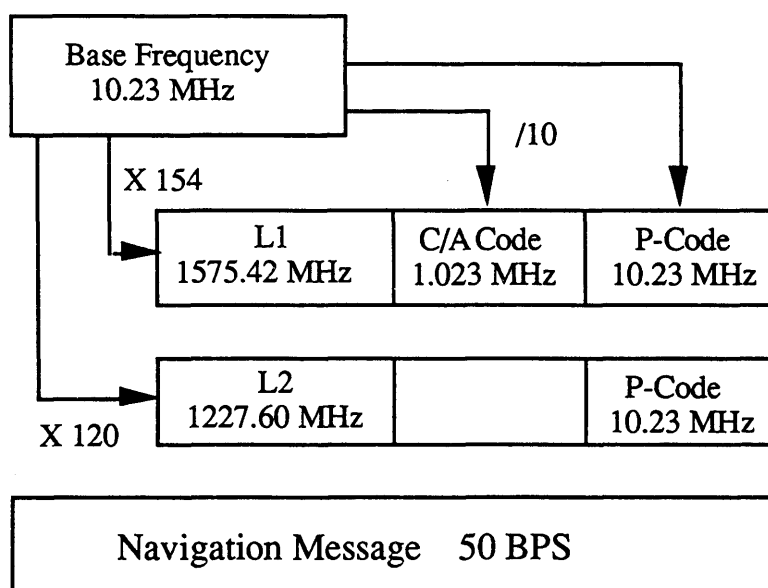


**Figure 2.1 Frequency and Signal Generation of GPS Satellite**

## 2.3 GPS OBSERVATIONS

Three different types of measurements can be taken when tracking a GPS satellite: (1) pseudorange measurement, (2) carrier beat phase measurement, and (3) instantaneous Doppler measurement.

**Pseudorange Measurement:** GPS satellites transmit signals which are labeled with the time of transmission given in the GPS time frame. Receivers measure the time of reception of the signal relative to the receiver clock. If the receiver clock is fully synchronized to GPS time, then the time difference between the transmission time and the reception time is exactly the travel time of the signal. Due to the fact that the satellite and receiver clocks are usually not synchronized, the range determined with this procedure is affected by clock synchronization error. These ranges are therefore referred to as pseudoranges.

The accuracy of pseudorange measurement depends on the Early/Late (E/L) correlator in the receiver Delay Lock Loops (DLLs) [Van Dierendonck et al., 1992]. Conventional GPS receivers use one chip correlation spacing. Measurements can be made to approximately 0.01 chip so that the noise on a C/A-code pseudorange is about 3 m, while that on P-code is 30 cm. Recently, many receivers are using some types of narrow Early/Late correlator spacing technology (e.g. NovAtel GPSCard<sup>TM</sup>, Trimble 4000SSE, Rogue SNR-8C, etc.). This technique allows GPS receivers to measure the pseudorange at a 10 cm noise level on C/A code [Van Dierendonck et al., 1992; Cannon and Lachapelle, 1992a].

**Carrier Beat Phase Measurement:** The carriers transmitted by satellites can be reconstructed in the receiver either by complete knowledge of the Pseudo-Random Codes (C/A-code or P-code) or by code-less signal processing

technology (e.g., squaring, cross-correlation). The phase of the incoming carriers is differenced with the phase of internally generated carriers. The difference is referred to as carrier beat phase. Today's receiver technology allows us to measure the carrier beat phase with an accuracy at the millimetre level, depending on the oscillator used in the receiver. These phases would represent the most accurate range measurements if the so-called initial phase ambiguity could be determined. The initial phase ambiguity is the unknown number of cycles between the satellite and the receiver at the epoch when the receiver locked onto the signal.

**Instantaneous Doppler Measurement:** Measurements can also be made with respect to the instantaneous Doppler frequency shift of the incoming carriers. This frequency shift is the result of the relative motion of the receiver and satellite, so it can be used to determine the velocity of a moving object [Cannon, 1990]. The accuracy of the instantaneous Doppler measurement depends on the receiver architecture and tracking bandwidth of the code tracking loop. Modern GPS receivers can measure the instantaneous Doppler frequency shift with an accuracy of 5 mm/second [Lachapelle et al., 1992b].

## 2.4 MAJOR ERROR SOURCES IN GPS OBSERVATIONS

GPS observations are subject to a number of errors, both random and systematic. The major error sources include receiver noise, orbital and clock errors, and propagation errors (ionospheric effect, tropospheric effect, and multipath). They are briefly discussed in this section. The ionospheric effect and multipath will be discussed in more detail in Chapter 4 and 5.

### 2.4.1 Orbital Errors

Orbital errors result from the situation where the satellite is not at the exact position dictated by the broadcast ephemerides. This discrepancy is the consequence of the inability to completely model the forces acting on a satellite, and the degradation due to Selective Availability (SA). If left uncorrected, such discrepancies will corrupt the range determination and hence the location of the user position. Differencing observations from one satellite between receivers can reduce the error. As a rule of thumb, the effect of orbital errors on baseline determination is [Vanicek et al., 1985]:

$$\frac{db}{b} = \frac{d\rho}{\rho} \quad (2.1)$$

where  $db$  is the error in baseline;  
 $b$  is the baseline length;  
 $d\rho$  is the orbital error;  
 and  $\rho$  is the satellite-receiver range.

Table 2.1 summarizes the acceptable orbital error for a given relative accuracy in baseline determination [Seeber, 1993].

**Table 2.1 Relative Accuracy and Orbital Errors**

Relative accuracy required	Acceptable orbital error
5 ppm	125 m
1 ppm	25 m
0.5 ppm	12.5 m
0.1 ppm	2.5 m

Another possibility to reduce the orbital error is to compute the *a posteriori* precise ephemerides, based on observations from globally distributed tracking stations. In addition to the U.S. military GPS satellite tracking networks, several civilian tracking networks are in the process of being established to determine the precise ephemerides [Seeber, 1993]. A well-known one is the Cooperative International GPS Network (CIGNET) with about 20 tracking stations operating in 1992.

#### **2.4.2 Clock Errors**

Clock errors occur in both the satellites and the receivers. Each satellite carries clocks which act as the time and frequency base for the realization of the GPS system time. Although the satellite clocks are very accurate, they are not perfect. The behavior of satellite clocks is monitored by the GPS ground control segment and the clock correction model is reported to the users as part of the navigation message. The actual behavior of the clock, however, differs from this model because of unpredictable, correlated frequency errors. Receiver clock drift is generally of larger than the satellite clock drift due to the lower quality of the oscillator.

Differencing observations from one satellite between two receivers can eliminate the satellite clock error. Differencing observations between satellites can eliminate the receiver clock error. An alternative approach is to leave the receiver and satellite clock offsets as an unknown to be solved in parameter estimation [Remondi, 1984].

The DoD is intentionally degrading the accuracy of position information to unauthorized users. This mode of degraded operation is called Selective

Availability (SA). SA involves the degradation of broadcast orbits and satellite clock dithering. Orbit degradation should not constitute a problem because high accuracy post-processing techniques routinely include orbit improvement calculations [Beutler et al., 1985]. Satellite clock dithering appears more problematic because it can result in unmodeled satellite clock errors. However, for the current level of SA, satellite clock dithering has a negligible effect on baselines determination if double difference processing techniques are employed and if the GPS receivers remain synchronized to better than 10 ms [Rocken et al., 1991].

### **2.4.3 Ionospheric Delay**

The atmospheric layer from about 60 km upwards is called the ionosphere and it includes free electrons. The ionosphere can retard GPS signals from their velocity in free space by more than 300 ns in the worst case, corresponding to range errors of 100 metres [Klobuchar, 1987]. The ionospheric delay depends on the Total Electron Content (TEC) along the signal path and on the frequency used. TEC is a function of solar ionizing flux, magnetic activity, user location, and viewing direction. Dual frequency receivers make use of the fact that the L1 and L2 signals experience different propagation delays in the ionosphere. However, the type of receivers used by the majority of civilian users will be of the less expensive, single frequency kind, which does not provide enough information to eliminate the delay. For precise positioning applications, some methods of reducing this error is highly desirable. In this thesis, one method of accomplishing this objective is proposed.

#### 2.4.4 Tropospheric Delay

The troposphere is the lowest part of the atmosphere, extending up to between 9 and 16 kilometres in altitude although the neutral atmosphere can extend up to several tens of kilometres. The tropospheric delay depends on the temperature, humidity, and pressure. It varies with the height of the user, and can also vary with the type of terrain below the signal path. The total tropospheric delay can be separated into a dry and a wet component [Hopfield, 1971]. The dry component, which reaches up to 90% of the total delay, is easier to determine than the wet component. Table 2.2 gives some numerical values of the tropospheric delay for different satellite elevation angles in average situation.

**Table 2.2 Tropospheric Delay on Measured Ranges**

Elevation	90°	20°	15°	10°	5°
Dry Component	2.3 (m)	6.7	8.8	12.9	23.6
Wet Component	0.2	0.6	0.8	1.1	2.2
Total Delay	2.5	7.3	9.6	14.0	25.8

Various models have been developed to estimate the delay. The dry component can be precisely described by these models with an accuracy of  $\pm 1\%$ , while the wet component can be modeled by surface weather data to within 3-4 cm [Wells, 1987]. Other approaches of determining the wet component include direct measurement with water vapor radiometers [Elgered et al., 1985] and the use of a station-dependent zenith scale factor for each satellite pass.

#### 2.4.5 Multipath

Multipath is the phenomena whereby a signal arrives at a receiver via multiple paths. Multipath propagation is almost inevitable in most GPS

applications, since all kinds of possible reflectors are normally present, such as the earth's surface, buildings and other objects. The influence of these reflections depends on their signal strength and delay compared with that of the line-of-sight signal, the attenuation by the receiver antenna, and the measuring technique of the receiver. The theoretical maximum effect of multipath on C/A code pseudorange measurements can reach 0.5 ms when the reflected/direct signal strength ratio is one. Carrier phase measurements are not free from multipath either. Though the effect is about two orders of magnitude smaller than in pseudoranges, it contributes to the phase measurement noise. For short baselines, it may even dominate the adjustment residuals in the solution. In a strong multipath environment, the observation time in the field may increase significantly in order to correctly resolve the satellite carrier phase ambiguities [Lachapelle et al., 1992c].

Multipath can be reduced by careful selection of observation site, and special design of receiver antenna and firmware [Meehan et al., 1992; Van Nee, 1992]. In some special cases, multipath can be predicted [Fu, 1992]. In this thesis, instead of modeling multipath, an attempt is made to estimate the observation time required for solving the carrier phase ambiguities in a strong multipath environment.

#### **2.4.6 Receiver Noise**

The receiver noise depends on the signal to noise ratio of the satellite signals. The dynamics acting on the antenna also have an effect. The greater the accelerations of the antenna, the wider the tracking loop bandwidths have to be in order to keep lock on a incoming signal, and the higher the noise level of the

receiver will be. As a rule of thumb, the observation resolution for classical receivers is slightly better than 1% of the signal wavelength. The typical receiver noise level is summarized in Table 2.3.

**Table 2.3 Receiver Noise for Different Observations**

Type of Obs.	Wavelength	Receiver Noise
C/A-code	300 m	3 m
P-code	30 m	30 cm
Carrier Phase	20 cm	2 mm

Modern receiver technology tends to bring the internal phase noise below 1 mm, and to reduce the code noise to the ten centimetre level [Van Dierendonck et al., 1992].

## CHAPTER 3

### RAPID STATIC GPS SURVEYS

The most accurate relative positioning performed with the Global Positioning System has resulted from carrier phase observations where the initial phase ambiguities are resolved and constrained to their correct integer values. Static GPS carrier phase relative positioning has yielded accuracies ranging from a few parts per million to a few parts per 100 million [Erickson, 1992; Lichten and Bertiger, 1989], depending on the observation and processing methodology used. Traditionally, site observation periods of at least one hour are typically recommended for short baselines (<10km) in order to achieve a few parts per million accuracy, with longer observation periods necessary for longer baselines. Efforts towards higher GPS surveying efficiency led to the development of rapid static positioning. As the name implies, rapid static GPS positioning involves a short static site occupation time of only a few minutes [Frei and Beulter, 1990].

During the past few years several techniques for rapid ambiguity resolution have been developed. These include "Extra-widelaning" [Wübbena, 1989; Abidin and Wells, 1990], "Sequential phase ambiguity resolution" [Talbot, 1991], the "Fast ambiguity resolution approach" [Frei and Beulter, 1990], the "Least Squares ambiguity search technique" [Hatch, 1991a; Lachapelle et al., 1992a], the "Ambiguity function method" [Counselman and Gourevitch, 1981; Remondi, 1984], and the "Fast Ambiguity Search Filter (FASF)" [Chen, 1993].

### 3.1 CARRIER PHASE RESOLUTION IN RAPID STATIC DGPS

The carrier phase measurement, as was discussed in Chapter 2, can be written as [Lachapelle, 1992d]:

$$\Phi = \rho + c(dt - dT) + \lambda \cdot N - d_{\text{ion}} + d_{\text{trop}} + d\rho + \varepsilon(\Phi) \quad (3.1)$$

where  $\Phi$  is the carrier phase measurement in metres;  
 $\rho$  is the geometric satellite-receiver range;  
 $d\rho$  is the orbit error;  
 $c$  is the speed of light in vacuum;  
 $dt$  is the satellite clock offset;  
 $dT$  is the receiver clock offset;  
 $\lambda$  is the wavelength of the carrier phase measurement;  
 $N$  is the unknown integer carrier phase ambiguity;  
 $d_{\text{ion}}$  is the ionospheric delay;  
 $d_{\text{trop}}$  is the tropospheric delay;  
 $\varepsilon(\Phi)$  is the receiver noise.

Because of difficulties in accurately modeling satellite orbits, clock errors, and propagation delays, double difference observations are formed from the combination of raw phase measurements between satellites and between receivers. Double difference observations are commonly used for differential precise positioning since it has the effect of eliminating or reducing many systematic errors inherent in raw phase measurements [Remondi, 1984]. The double difference observation equation for carrier phase is:

$$\nabla\Delta\Phi = \nabla\Delta\rho + \lambda \cdot \nabla\Delta N - \nabla\Delta d_{\text{ion}} + \nabla\Delta d_{\text{trop}} + \nabla\Delta d\rho + \varepsilon(\nabla\Delta\Phi) \quad (3.2)$$

where  $\nabla\Delta$  is the double difference operator. The unknown remote station coordinates  $(X, Y, Z)$  are contained in  $\nabla\Delta\rho$ . The difficulty in resolving remote station coordinates and ambiguity terms simultaneously is due to the similarity of  $\nabla\Delta\rho$  and  $\nabla\Delta N$ , both of which are range related. Separation of the coordinates from the ambiguities requires a significant change in satellite geometry resulting from relative satellite motion.

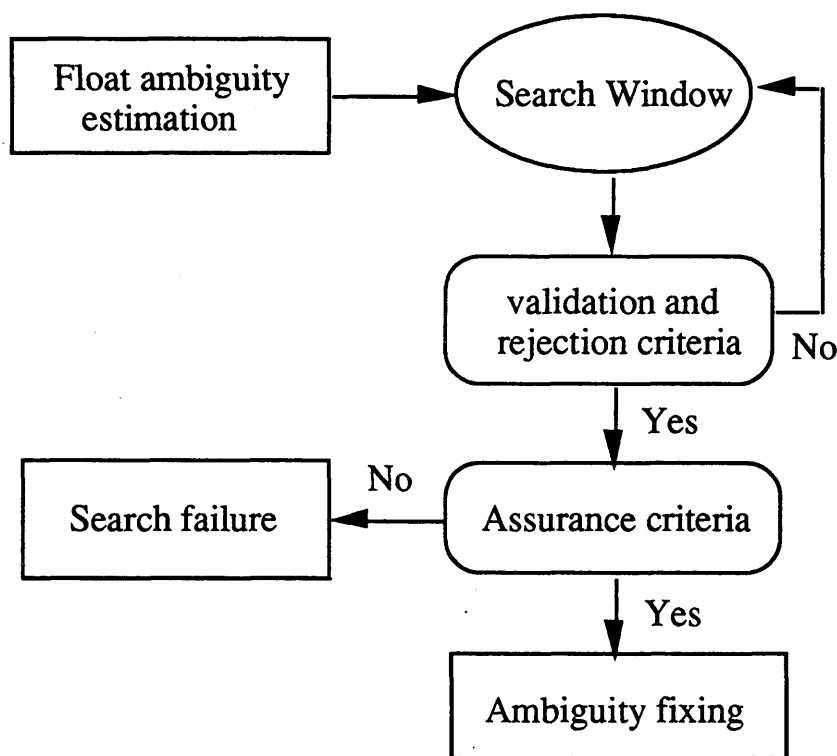


**Figure 3.1 General Strategy for Rapid Static Ambiguity Resolution**

All rapid static ambiguity resolution techniques have a more or less similar strategy for resolving ambiguities. Basically, the procedure starts with an estimation of initial remote coordinates or initial ambiguities. The ambiguity resolution is performed by testing many combinations of potential ambiguity sets inside a certain predetermined searching space. Each potential ambiguity set is

tested by applying certain validation and rejection criteria. The searching process is stopped and the ambiguities are fixed when certain assurance criteria are fulfilled. This procedure is summarized in Fig. 3.1.

The more satellites are available, the better the searching procedure works since each additional satellite restricts the number of possible solutions. In the following sections, the general strategy for rapid static ambiguity resolution procedure is discussed in more detail.

### 3.1.1 Carrier Phase Ambiguity Float Solution

As a first step, a fast ambiguity resolution algorithm normally involves the computation of a double difference carrier float solution following the observation equation (3.2). The linearized form of equation (3.2) is:

$$\underline{V} = \underline{A}\underline{X} + \underline{W} \quad (3.3)$$

where  $\underline{V}$  is the vector of residuals;  $\underline{A}$  is the design matrix, the explicit form of which is given in [Erickson, 1992];  $\underline{W}$  is the misclosure vector; and  $\underline{X}$  is the state vector containing the unknown remote station coordinates and carrier phase ambiguities:

$$\underline{X} = [X, Y, Z, \nabla\Delta N_1, \nabla\Delta N_2, \dots, \nabla\Delta N_{nsat-1}]$$

where nsat is the number of satellites being tracked during the observation. The corresponding least-squares solution of the estimated state vector  $\hat{\underline{X}}$  is:

$$\hat{\underline{X}} = -(\underline{A}^T \underline{C}_1^{-1} \underline{A})^{-1} \underline{A}^T \underline{C}_1^{-1} \underline{W} \quad (3.4)$$

and the adjusted residuals,  $\hat{\underline{V}}$ , are computed as:

$$\hat{\underline{V}} = \underline{A}\hat{\underline{X}} + \underline{W} \quad (3.5)$$

where  $\underline{C}_1$  is the covariance matrix of the observations [Krakiwsky, 1990].

Since the a priori variance factor is unknown beforehand,  $\underline{C}_1$  is derived using a unit *a priori* variance factor, and the *a posteriori* variance factor,  $\hat{\sigma}_0^2$ , is estimated as:

$$\hat{\sigma}_0^2 = \frac{\hat{\underline{V}}^T \underline{C}_1^{-1} \hat{\underline{V}}}{n - u} \quad (3.6)$$

where  $n$  is the number of observations and  $u$  is the number of unknown parameters. The covariance matrix of the adjusted parameters is scaled by the a posteriori variance factor to give:

$$\hat{\underline{C}}_{\hat{\underline{X}}} = \hat{\sigma}_0^2 \underline{C}_{\hat{\underline{X}}}$$

where  $\hat{\underline{C}}_{\hat{\underline{X}}}$  is the estimation of the covariance matrix of the adjusted parameters  $\underline{C}_{\hat{\underline{X}}}$ .

### 3.1.2 Ambiguity Searching Window

In the second step, the searching space of potential integer ambiguities is defined. The searching space could be either the mathematical space (defined in the ambiguity domain) or the physical space (defined in the position domain). The searching technique in physical space is discussed in [Remondi, 1984]. Since searching in mathematical space is more efficient than in physical space, only searching in mathematical space is discussed here. There are many possibilities to define the integer ambiguity search ranges [Abidin, 1993; Frei, 1991]. One approach is to determine the integer ambiguity ranges based on the confidence

intervals around the real ambiguity solutions using the appropriate diagonal components of  $\hat{\underline{C}}_{\hat{\underline{X}}}$  [Frei, 1991]. Letting  $\hat{N}_j$  represent an estimated real ambiguity from the float solution and  $N_j^P$  a potential integer value for the same ambiguity, then

$$P\{\hat{N}_j - \xi_{t,df,1-\alpha/2} \cdot \sigma_{N_j} \leq N_j^P \leq \hat{N}_j + \xi_{t,df,1-\alpha/2} \cdot \sigma_{N_j}\} = 1 - \alpha \quad (3.7)$$

where  $P\{ \}$  represents the probability for a certain confidence level  $1-\alpha$ ,  $\xi_{t,df,1-\alpha/2}$  is the student t distribution for  $df$  degrees of freedom and a significant level of  $\alpha$ , and  $\sigma_{N_j}$  is the standard deviation of the float ambiguity  $\hat{N}_j$ .

In order to reduce the potential ambiguity sets in searching space, the observed satellites can be divided into two groups, i.e., primary satellites and secondary satellites [Hatch, 1991a] by the fact that the ambiguities corresponding to the four primary satellites mathematically determine the other ambiguities corresponding to the remaining satellites. Therefore, it is only necessary to search for the primary ambiguities regardless of the number of satellites. The advantage of this technique is that only a three-dimensional searching space needs be considered.

### 3.1.3 Testing of Integer Ambiguity Combinations

After constructing the ambiguity searching space, the next step is to try to identify the correct ambiguities from the potential ambiguity sets inside the searching space by applying certain validation and rejection criteria. Some of these criteria are:

(1) *Compatibility test between potential coordinates and the code-derived coordinates.*

The potential position is computed as if the carrier phase ambiguities were exactly known. If the potential ambiguities are correct, then the corresponding estimated position should differ from the code-derived position in a statistically predictable manner. The differences in coordinates in this case will be caused only by the differences in precision between code and phase observations. This criterion can be formulated as [Abidin, 1993]:

$$|\hat{\underline{X}}_P - \hat{\underline{X}}_C| < \mathfrak{R}(0,1)_{1-\alpha/2} \cdot \hat{\sigma}_{\hat{\underline{X}}_C} \quad (3.8)$$

where  $\hat{\underline{X}}_P$  is the potential position,  $\hat{\underline{X}}_C$  is the code-derived position,  $\mathfrak{R}(0,1)_{1-\alpha/2}$  is the Gaussian normal distribution with the confidence level  $1-\alpha$ , and  $\hat{\sigma}_{\hat{\underline{X}}_C}$  is the standard deviation of the code-derived position. The compatibility test between potential position and code-derived position is especially useful when very precise code measurements are used.

(2). *Ambiguity function test of the adjusted residuals.* The ambiguity function  $AF(\hat{\underline{X}}_P)$  for the potential position  $\hat{\underline{X}}_P$  is defined as [Remondi, 1984]:

$$AF(\hat{\underline{X}}_P) = \text{REAL} \left( \sum_{k=1}^{\text{nepoch}} \sum_{j=1}^{\text{nsat}-1} e^{2\pi i (\nabla \Delta \Phi_{\text{obs}}^{kj} - \nabla \Delta \rho_{\text{calc}}^{kj}(\hat{\underline{X}}_P))} \right) \quad (3.9)$$

where  $\nabla \Delta \Phi_{\text{obs}}^{kj}$  is the observed double difference range,  $\nabla \Delta \rho_{\text{calc}}^{kj}(\hat{\underline{X}}_P)$  is the computed double difference range for the potential position  $\hat{\underline{X}}_P$ ,  $\text{nsat}$  is the number of satellites observed, and  $\text{nepoch}$  is the number of epochs. Summations are made for all  $(\text{nsat}-1)$  double difference observations and all epochs. The normalized ambiguity function  $\overline{AF}(\hat{\underline{X}}_P)$  is:

$$\overline{AF}(\hat{\underline{X}}_P) = \frac{1}{\text{nepoch} \cdot (\text{nsat} - 1)} AF(\hat{\underline{X}}_P) \quad (3.10)$$

The ambiguity mapping function measures the agreement between the measurements and their calculated values. The ambiguity function will have a maximum value when the phase residual is calculated at the correct potential position, or at all other candidate positions where the double difference residual changes by an integer number of wavelengths. This leads to the criterion of ambiguity function testing:

$$\overline{AF}(\hat{X}_p) > \text{minimum threshold} \quad (3.11)$$

(3). *Compatibility test between pair of ambiguities.* This test makes FARA unique as compared to other rapid static ambiguity resolution techniques [Frei, 1991; Erickson, 1992]. In each set of potential ambiguity solutions, pairs of ambiguities are tested. The differences between two real ambiguities and the difference between corresponding potential integer ambiguities are formed as:

$$\nabla\Delta N_{ij} = \nabla\Delta N_i - \nabla\Delta N_j \quad (3.12a)$$

$$\nabla\Delta N_{ij}^f = \nabla\Delta N_i^f - \nabla\Delta N_j^f \quad (3.12b)$$

The standard deviation of the real ambiguity difference  $\nabla\Delta N_{ij}^f$  is:

$$\sigma_{N_{ij}^f} = \sqrt{\sigma_{N_i^f}^2 + \sigma_{N_j^f}^2 - 2\sigma_{N_i^f N_j^f}} \quad (3.13)$$

where  $\sigma_{N_i^f}$ ,  $\sigma_{N_j^f}$  and  $\sigma_{N_i^f N_j^f}$  can be obtained from  $\hat{C}_{\hat{X}}$ .

The criterion relating the real ambiguity differences with potential integer ambiguity differences is then written as:

$$P\{N_{ij}^f - \xi_{t,df,1-\alpha/2} \cdot \sigma_{N_{ij}^f} \leq N_{ij} \leq N_{ij}^f + \xi_{t,df,1-\alpha/2} \cdot \sigma_{N_{ij}^f}\} = 1 - \alpha \quad (3.14)$$

Ambiguity sets with pairs of ambiguities which do not fulfill equation (3.14) are rejected from consideration.

(4). *Test on the quadratic form of the residuals.* The quadratic form of the residuals  $\underline{V}^T \underline{C}_1^{-1} \underline{V}$  is the quantity which is to be minimized by the adjustment process. If the correct ambiguities are involved, and assuming that only the random errors are present in the observations, then the value of the quadratic form of the residuals should be statistically predictable and smaller than a certain threshold. In this case, one-sided statistical Chi-squared testing is applied, and the criteria is formulated as:

$$\frac{\underline{V}^T \underline{C}_1^{-1} \underline{V}}{\sigma_0^2} \leq \xi_{\chi^2, df, 1-\alpha} \quad (3.15)$$

where  $\sigma_0^2$  denotes the *a priori* variance factor and  $\xi_{\chi^2, df, 1-\alpha}$  is the Chi-squared distribution with *df* degree of freedom and confidence level  $(1-\alpha)$ .

Many other criteria can also be employed in this step [Abidin, 1993]. Some of these criteria are mathematically equivalent [Lachapelle et al., 1992e]. In fact, rapid static ambiguity resolution techniques usually differ from each other in these validation and rejection criteria used in the searching process. These differences usually lead to the differences in computation and observation time in ambiguity resolution and sometimes in the reliability of resolution.

### 3.1.4 Assurance of The Integer Ambiguity

The searching process of the integer ambiguity set is stopped if only one potential ambiguity set survives all validation and rejection criteria. However, this ambiguity set could be either the correct integers or the incorrect ones. Fixing

the ambiguities to the incorrect integers could be caused by several factors. Insufficient observation time is one of them. Other factors include the use of parameters in validation and rejection criteria which do not represent the realistic level of random and systematic errors.

If more than one potential ambiguity set passes these validation and rejection criteria, a choice has to be made to select the correct ambiguity set. One commonly used criterion is to choose the ambiguity set which yields the smallest variance factor as the correct integers. In this case, the smallest and the next smallest variance factor are compared to ensure their independence. The comparison is given as [Erickson, 1992]:

$$\frac{\hat{\sigma}_2}{\hat{\sigma}_1} \geq \xi_{F,df1,df2,\alpha} \quad (3.16)$$

where  $\hat{\sigma}_1$  is the smallest variance factor,  $\hat{\sigma}_2$  is the second smallest variance factor, and  $\xi_{F,df1,df2,\alpha}$  is the F (Fisher) distribution for df1 degrees of freedom (for the solution with the smallest variance factor) and df2 degrees of freedom (for the solution with the second smallest variance factor) and with a significant level  $\alpha$ . If the ambiguity set with the smallest variance factor fails the test of equation (3.16), the observation data is deemed to be insufficient to correctly resolve the ambiguity.

### 3.1.5 A Fast Quadratic Form Testing Algorithm

Ideally, all possible potential ambiguity sets inside the searching space should be tested to ensure the correct ambiguities are included. The basic problem is that the number of necessary mathematical operations increases rapidly as the

searching space grows. For example, if there are 6 unknown integer ambiguities, each one known to  $\pm 10$  cycles, then there are  $(21^6)$  possible combinations to be tested. Many rapid static ambiguity resolution algorithms require computing a batch least-squares solution for each potential ambiguity set to obtain the variance factor  $\hat{\sigma}_0^2$  for the quadratic form testing, thus consuming enormous computer time. Langley et al. [1984] developed a fast algorithm to calculate the quadratic form of residuals, which was further improved by Landau and Euler [1992]. The algorithm is described in this section.

Let us divide the unknown state vector  $\underline{X}$  into two parts:

$$\underline{X} = [\underline{X}_1, \underline{X}_2] \quad (3.17)$$

where  $\underline{X}_1 = [X, Y, Z]$  contains the coordinates of remote station,  $\underline{X}_2 = [\nabla\Delta N_1, \nabla\Delta N_2, \dots, \nabla\Delta N_u]$  is the double difference ambiguities. and  $u$  is the number of unknown ambiguities to be resolved.

The observation equation (3.3) can be rewritten as:

$$\underline{V} = \underline{A}_1 \underline{X}_1 + \underline{A}_2 \underline{X}_2 + \underline{W} \quad (3.18)$$

where  $\underline{A}_1$  is the sub-matrix formed with the first three columns of the design matrix  $\underline{A}$ ,  $\underline{A}_2$  is the sub-matrix formed with the last  $u$  columns of  $\underline{A}$ . Equation (3.4) may be rewritten as:

$$\begin{bmatrix} \underline{A}_1^T \underline{C}_1^{-1} \underline{A}_1 & \underline{A}_1^T \underline{C}_1^{-1} \underline{A}_2 \\ \underline{A}_2^T \underline{C}_1^{-1} \underline{A}_1 & \underline{A}_2^T \underline{C}_1^{-1} \underline{A}_2 \end{bmatrix} \begin{bmatrix} \hat{\underline{X}}_1 \\ \hat{\underline{X}}_2 \end{bmatrix} = - \begin{bmatrix} \underline{A}_1^T \underline{C}_1^{-1} \\ \underline{A}_2^T \underline{C}_1^{-1} \end{bmatrix} \underline{W} \quad (3.19)$$

Introducing

$$N_{11} = \underline{A}_1^T \underline{C}_1^{-1} \underline{A}_1, \quad N_{12} = \underline{A}_1^T \underline{C}_1^{-1} \underline{A}_2, \quad N_{22} = \underline{A}_2^T \underline{C}_1^{-1} \underline{A}_2 \quad (3.20)$$

and

$$\underline{U}_1 = -\underline{A}_1^T \underline{C}_1^{-1} \underline{W}, \quad \underline{U}_2 = -\underline{A}_2^T \underline{C}_1^{-1} \underline{W} \quad (3.21)$$

then equation (3.19) becomes:

$$\begin{bmatrix} N_{11} & N_{12} \\ N_{12}^T & N_{22} \end{bmatrix} \begin{bmatrix} \hat{X}_1 \\ \hat{X}_2 \end{bmatrix} = \begin{bmatrix} \underline{U}_1 \\ \underline{U}_2 \end{bmatrix} \quad (3.21)$$

The least-squares solution of  $\hat{X}_1$  is

$$\hat{X}_1 = N_{11}^{-1} (\underline{U}_1 - N_{12} \hat{X}_2) \quad (3.22)$$

Let  $\underline{X}_2^*$  be a new set of potential ambiguities instead of  $\hat{X}_2$ . We are now looking for the best approximation of  $\hat{X}_1$  in the least-squares sense, provided  $\hat{X}_2$  is approximated by  $\underline{X}_2^*$ . The solution is:

$$\hat{X}_1^* = N_{11}^{-1} (\underline{U}_1 - N_{12} \underline{X}_2^*) \quad (3.23)$$

The new value of residuals vector  $\underline{V}^*$  is then:

$$\begin{aligned} \underline{V}^* &= \underline{A}_1 \hat{X}_1^* + \underline{A}_2 \underline{X}_2^* - \underline{W} \\ &= \underline{A}_1 N_{11}^{-1} (\underline{U}_1 - N_{12} \underline{X}_2^*) + \underline{A}_2 \underline{X}_2^* - \underline{W} \end{aligned} \quad (3.24)$$

The quadratic form of the residuals becomes:

$$\underline{V}^{*T} \underline{C}_1^{-1} \underline{V}^* = \underline{W}^T \underline{C}_1^{-1} \underline{W} + D_1 + \underline{D}_2^T \underline{X}_2^* + \underline{X}_2^{*T} \underline{D}_3 \underline{X}_2^* \quad (3.25)$$

where  $D_1 = -\underline{U}_1^T N_{11}^{-1} \underline{U}_1$  is a constant,  $\underline{D}_2^T = -2(\underline{U}_2^T - \underline{U}_1^T N_{11}^{-1} N_{12})$  is a vector, and

$\underline{D}_3 = (N_{22} - N_{12}^T N_{11}^{-1} N_{12})$  is a symmetric matrix. As  $D_1$ ,  $\underline{D}_2$  and  $\underline{D}_3$  are functions of components in equation (3.21), once the ambiguity float solution has been carried out, all of them become constant and, therefore, only need to be calculated once. The quadratic form of residuals corresponding to each potential ambiguity set can be obtained from equation (3.25) without carrying out the least-squares adjustment.

The above ambiguity searching procedure can be further improved by applying the Cholesky decomposition of the symmetric matrix  $\underline{D}_3$ :

$$\underline{D}_3 = \underline{L}\underline{L}^T \quad (3.26)$$

where  $\underline{L}$  is a lower triangular matrix. Substituting equation (3.26) into equation (3.25) leads to the following simple results:

$$\begin{aligned} \underline{V}^{*T} \underline{C}_1^{-1} \underline{V}^* &= \underline{W}^T \underline{C}_1^{-1} \underline{W} + D_1 + \underline{D}_2^T \underline{X}_2^* + (\underline{X}_2^{*T} \underline{L})(\underline{L}^T \underline{X}_2^*) \\ &= \underline{W}^T \underline{C}_1^{-1} \underline{W} + D_1 + \underline{D}_2^T \underline{X}_2^* + \underline{Y}^T \underline{Y} \end{aligned} \quad (3.27)$$

where  $\underline{Y} = \underline{L}^T \underline{X}_2^*$  is a vector. Instead of performing the complete matrix multiplication, equation (3.27) breaks down to a much faster vector multiplication.

### 3.2 THE INFLUENCE OF SATELLITE GEOMETRY ON AMBIGUITY RESOLUTION

In rapid static surveying, whether initial ambiguities can be resolved or not depends on a few rather complex factors, e.g. the satellite geometry, the type and quality of measurements available, the effects of systematic errors, etc. The site occupation periods are usually set based on experience and conservative rules-

of-thumb. However, on occasions post processing reveals that the results of a survey session do not meet the required accuracy standard, and the session must be re-observed.

Real-time positioning offers a potential means of improving the efficiency of static positioning. In this case, a field operator can be signaled when all ambiguities are resolved and baseline precision has reached a predefined tolerance. Site occupation time can, therefore, be reduced to a minimum [Talbot, 1991].

Since the capabilities of real-time GPS data communication are still limited, a reliable and accurate algorithm to predict the site occupation time required to resolve the ambiguities is highly desirable. Prediction algorithms have been proposed by several authors, e.g. the "Resolution of the cycle ambiguity" [Mermind, 1988] and the "Rapid differential Positioning with the Global Positioning System (GPS)" [Frei, 1991]. Most of them are based on the variance-covariance analysis of the estimated ambiguities. In the following section, an ambiguity resolution prediction algorithm by sequential variance-covariance analysis is described.

### 3.2.1 Ambiguity Resolution Prediction Algorithm

Sequential processing of double difference carrier phase measurements can be easily derived from Kalman filter as a special case. The general Kalman filter equations are well documented in [Gelb, 1974]. For a system described by the following equations:

$$\underline{X}_k = \underline{\Phi}_k \underline{X}_{k-1} + \underline{w}_k, \quad \underline{w}_k \sim N(0, \underline{Q}_k) \quad (3.28)$$

$$\underline{Z}_k = \underline{A}_k \underline{X}_k + \underline{e}_k, \quad \underline{e}_k \sim N(0, \underline{R}_k), \quad (3.29)$$

the optimal estimate of the vector  $\underline{X}_k$  and its covariance matrix are given by:

$$\hat{\underline{X}}_k(-) = \underline{\Phi}_k \hat{\underline{X}}_{k-1}(+) \quad (3.30)$$

$$\underline{P}_k(-) = \underline{\Phi}_k \underline{P}_{k-1}(+) \underline{\Phi}_k^T + \underline{Q}_k \quad (3.31)$$

$$\hat{\underline{X}}_k(+) = \hat{\underline{X}}_k(-) + \underline{K}_k [\underline{Z}_k - \underline{A}_k \hat{\underline{X}}_k(-)] \quad (3.32)$$

$$\underline{P}_k(+) = [\underline{I} - \underline{K}_k \underline{A}_k] \underline{P}_k(-) \quad (3.33)$$

$$\underline{K}_k = \underline{P}_k(-) \underline{A}_k^T [\underline{A}_k \underline{P}_k(-) \underline{A}_k^T + \underline{R}_k]^{-1} \quad (3.34)$$

- where
- (-) denotes the predicted quantities,
  - (+) denotes the updated quantities,
  - $\underline{X}_k$  is the state vector,
  - $\underline{\Phi}_k$  is the transition matrix,
  - $\underline{P}_k$  is the state covariance matrix,
  - $\underline{K}_k$  is the Kalman gain matrix,
  - $\underline{Q}_k$  is the covariance matrix of the system process noise  $\underline{w}_k$ ,
  - $\underline{R}_k$  is the covariance matrix of the observation noise  $\underline{e}_k$ ,
  - $\underline{A}_k$  is the design matrix, and
  - $\underline{Z}_k$  is the observation vector at epoch k.

Since no actual measurements are needed in the variance-covariance analysis of initial ambiguities, only equations (3.31), (3.33) and (3.34) need to be calculated in the ambiguity resolution prediction algorithm. In the case of rapid static surveying with double difference carrier phase measurements, the transition matrix  $\underline{\Phi}_k$  is simply a identity matrix, and the covariance matrix of system

process noise  $\underline{Q}_k$  is a null matrix. This leads to the following recursive equations for the variance-covariance analysis of the initial ambiguities:

$$\underline{P}_k = [\underline{I} - \underline{K}_k \underline{A}_k] \underline{P}_{k-1} \quad (3.35)$$

$$\underline{K}_k = \underline{P}_{k-1} \underline{A}_k^T [\underline{A}_k \underline{P}_{k-1} \underline{A}_k^T + \underline{R}_k]^{-1} \quad (3.36)$$

The design matrix  $\underline{A}_k$  at epoch  $k$  is described in [Erikson, 1992]. The observation noise covariance matrix has the following form [Remondi, 1984]:

$$\underline{R}_k = \sigma_0^2 \begin{bmatrix} 4 & 2 & \dots & 2 \\ 2 & 4 & \dots & 2 \\ \dots & \dots & \dots & \dots \\ 2 & 2 & \dots & 4 \end{bmatrix} \quad (3.37)$$

where  $\sigma_0^2$  is the *a priori* carrier phase measurement variance.

In the ambiguity resolution prediction algorithm, the formal precision for each ambiguity term is analysed at each epoch and a decision to fix a given term is made once its formal precision drops below a preset tolerance:

$$\text{Fix ambiguity } \nabla \Delta N_i \text{ if } \hat{\sigma}_{\nabla \Delta N_i}^2 < \text{threshold} \quad (3.38)$$

If the ambiguity is successfully fixed, this ambiguity can be constrained by enforcing a small number ( $10^{-8}$  cycles<sup>2</sup>) on the variance element and zeros on the covariance elements that the ambiguity involves in the matrix  $\underline{P}_k$ . Constraint of one ambiguity improves the estimation of the other ambiguities. This is due to the mathematical correlation that exists in the double differences that share a reference satellite. Once the formal precision of all the ambiguities drop below the preset threshold, it is assumed that this particular satellite geometry will result in successful ambiguity resolution.

### 3.2.2 Numerical Results

To prove the validity of such an ambiguity resolution prediction approach, two tests with actual measurements taken under different satellite constellations and with different receivers were conducted.

In the first test, a 442 m baseline was observed with Ashtech P-XII receivers near Springbank Airport west of Calgary on August 20, 1992. Metal chokering ground planes were used at both the monitor and remote locations to minimize multipath. One hour of data were recorded during which 6 satellites were tracked using a 15° degree cutoff angle. The satellite elevation angles for this period are shown in Table 3.1.

**Table 3.1 Satellite Elevation Angles for 442 m Baseline Data**

SV	Elevation Angle (start to end, degrees)
11	27-49
17	45-19
21	57-82
23	78-52
26	22-15
28	20-35

The L1 carrier phase measurements of this data set were analysed using the above algorithm. The threshold in equation (3.38) was set to 3 cm (15% of the wavelength). The formal precisions of the ambiguity parameters for the 442 m baseline are shown in Figure 3.2. The combination SV26-SV23 displays a standard deviation which is significantly less than the other four ambiguities and is the first one resolved. Overall convergence of the remaining ambiguities is

benefiting from the constraint of this ambiguity. This can be deduced from the marked drop of the formal precision after epoch 240 seconds. The remaining ambiguities are all isolated within 280 seconds.

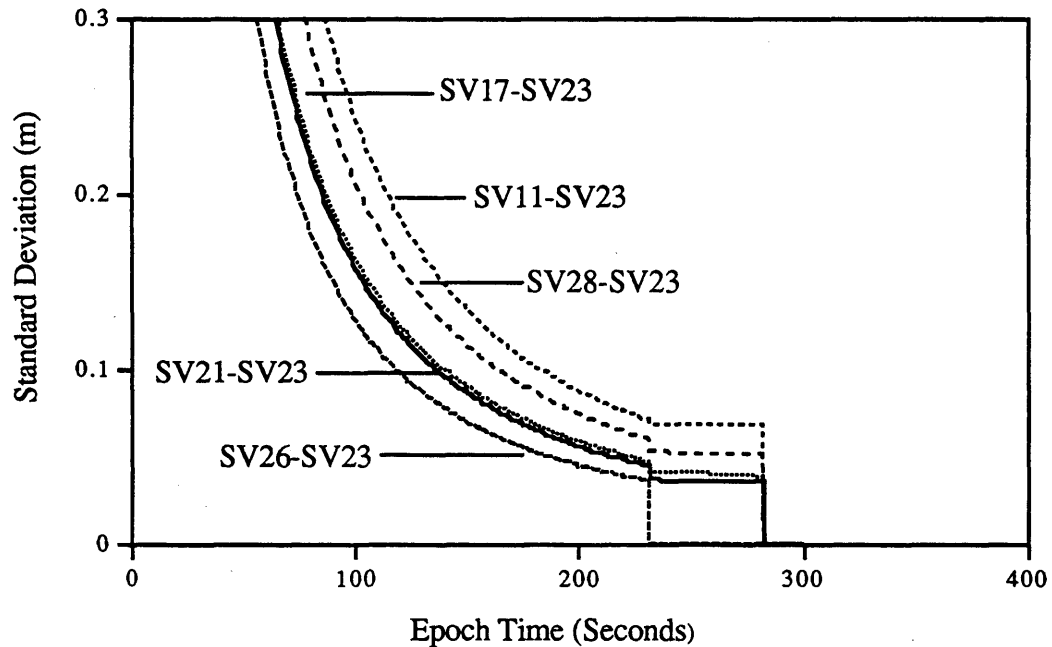


**Figure 3.2 Evolution of Formal Phase Ambiguity Precision  
for 442m Baseline (L1)**

The entire data set was then processed using the rapid static ambiguity resolution techniques discussed in this chapter. Fourteen trials, each using 280 seconds of data were tested to determine the site occupation time needed to resolve the ambiguities. Table 3.2 shows the results of the rapid static test. For each of the fourteen trials, two statistical measures are displayed; 1) the ratio of the second smallest sum-of-squares to the smallest sum-of-squares, and 2) the RMS of fit of the carrier phase residuals from the double difference fixed

processing. These two measures are important since they represent the quality of the rapid static solution. The larger the ratio of the sum-of-squares, the higher the statistical certainty of correct integer ambiguity selection. The smallest the RMS of fit, the better the solution. In this test, the correct integer ambiguities were achieved in 13 out of 14 trials.

**Table 3.2 Rapid Static Test Results for 442m Baseline**

TRIAL NO.	RATIO	RMS (mm)	RDOP
1	15.482	1.0	0.204
2	24.760	2.0	0.193
3	48.375	1.0	0.182
4	20.070	1.0	0.174
5	13.124	1.0	0.206
6	6.334	1.0	0.206
7	11.276	1.0	0.207
8	6.041	1.0	0.210
9	1.032*	1.6	0.192
10	4.546	2.0	0.170
11	6.484	2.0	0.176
12	10.813	2.0	0.184
13	8.444	2.0	0.192
14	5.908	2.0	0.200

\* Integer ambiguities are assumed not reliably determined.

In the second test, a 519 m baseline was observed with NovAtel GPSCard™ receivers near Fort Belvoir, USA on December 7, 1992 [Lachapelle et al., 1993]. No chokerings were used. Six satellites were tracked in the analyzed data segment. The satellite elevation angles during this period are shown in Table 3.3.

**Table 3.3 Satellite Elevation Angles for 519 m Baseline Data**

SV	Elevation Angle (start to end, degrees)
3	20-15
12	33-50
17	80-60
21	30-45
23	70-75
26	46-17

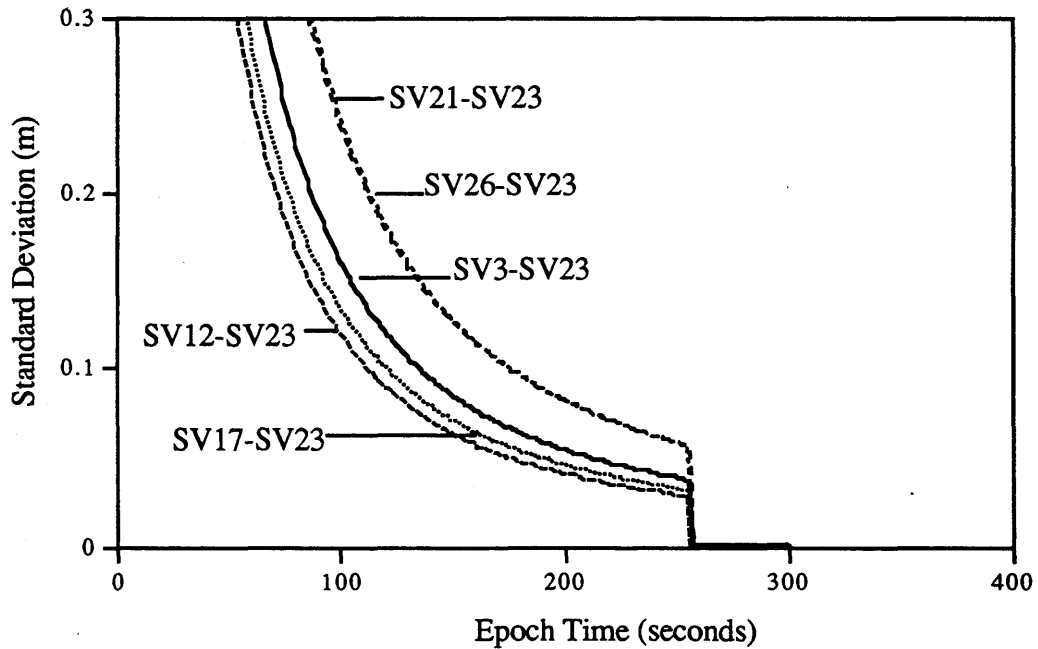


**Figure 3.3 Evolution of Formal Phase Ambiguity Precision  
for 519 m Baseline (L1)**

The formal precisions of the ambiguity parameters from the ambiguity resolution prediction algorithm using the same threshold are shown in Figure 3.3. The pre-analysis indicates that after 250 seconds of observation time, all the ambiguities can be successfully resolved. This data segment was then processed

in rapid static mode. Ten trials each using 250 seconds of observations were tested. The results are shown in Table 3.4.

**Table 3.4 Rapid Static Test Results for 519m Baseline**

Trial No.	Ratio	RMS (mm)	RDOP
1	1.323*	10.1	0.129
2	3.206	5.0	0.137
3	6.512	4.0	0.141
4	1.275*	11.0	0.134
5	3.160*	14.8	0.148
6	1.268*	15.7	0.157
7	1.621*	8.0	0.153
8	2.066	9.0	0.148
9	1.350*	8.0	0.152
10	2.034	4.0	0.144

\* Integer ambiguities are assumed not reliably determined.

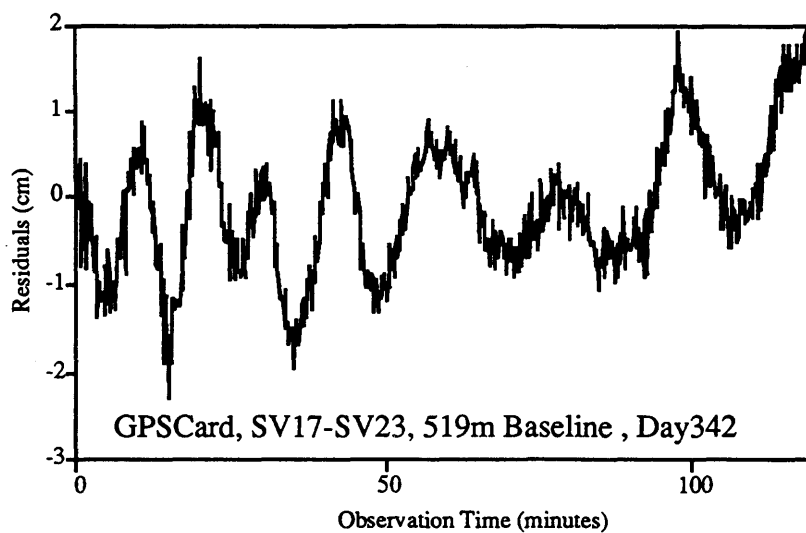


**Figure 3.4 Double Difference Residuals of Satellite Pair SV17-SV23  
for 519 m Baseline (L1)**

As it can be seen from Table 3.4, the success rate of trials in which ambiguities are correctly resolved is not high. Further analysis reveals that multipath is one of the major factors which affects the observation time needed to resolve the ambiguities. The double difference carrier phase residuals of the satellite pair SV17-SV23 are shown in Figure 3.4. The periodic characteristics of the residuals clearly indicate the presence of strong multipath.

From these two tests we may conclude that:

(1). The ambiguity resolution prediction algorithm can be employed in real-time to inform the user when sufficient measurements have been taken to resolve the ambiguities in rapid static surveys. The algorithm is simple and self-contained. Under favorable conditions (low multipath environment), the success rate of this predictor is very high.

(2). The use of such a predictor without using any actual measurements has some severe limitations. One has to assume that every available satellite can actually be tracked by all the participating receivers. The procedure relies on the assumption that the actual noise level in the measurements is very close to the *a priori* one assigned to the algorithm. However, carrier phase multipath will strongly degrade the data quality and thus affect the site occupation time needed to resolve the ambiguities.

## CHAPTER 4

### MULTIPATH EFFECT ON RAPID STATIC DGPS

Multipath is the phenomenon whereby a signal arrives at a receiver via multiple paths. Multipath is mainly caused by reflections. Due to the reflection of nearby objects such as ground streets, buildings, waterways and vehicles, the received signal will be composed of the direct line of sight signal and one or more indirect (reflected) signals, as is depicted in Figure 4.1. Purely from geometry it is clear that signals received from low satellite elevations are more susceptible to this kind of multipath than signals from high elevations. Since both the antenna and the reflect objects are stationary in rapid static surveys, multipath errors in pseudorange and carrier phase have periodic characteristics due to the changing satellite geometry. This kind of multipath is critical to rapid static surveys as well as kinematic positioning.

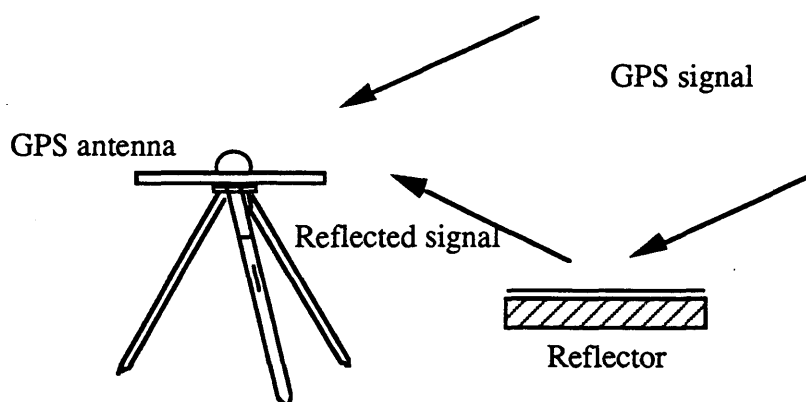


Figure 4.1 Multipath Caused by Reflection

Multipath affects both pseudorange and carrier phase measurements. Multipath error in pseudorange measurements has been studied for almost two decades. In 1973, Hagerman derived the relationships involving multipath and code tracking [Hagerman, 1973]. This fundamental work formed the basis for the analysis of GPS code and carrier multipath errors. Early studies indicated that [Bishop et al., 1985]:

(1). Multipath can cause both increases and decreases in delay depending on the relative phase of the reflected signal to the direct signal.

(2). The magnitude of the multipath error depends on the relative strength of the reflected signal to the direct signal. The theoretical maximum delay error can reach 150 m for C/A-code pseudoranges when the reflected/direct signal ratio is one.

(3). Typical multipath errors show sinusoidal oscillations of periods of 6-10 minutes and a magnitude of 9 metres or less.

Various ways of reducing multipath errors have been investigated. Performance improvements were obtained by mounting the antenna on radio frequency (RF) absorbent material and thereby improving the characteristics of the antenna pattern. Lachapelle et al. [1989] described marine DGPS experiments in which multipath was mitigated through the use of RF absorbing ground planes and filtering schemes. Evans [1986] demonstrated multipath effects on ionospherically corrected code and carrier phase measurements from geodetic receivers. Georgiadou and Kleusberg [1988a] considered multiple reflections and showed that multipath on short baselines could be detected using dual frequency measurements. Abidin [1990] examined the effects of multipath on ambiguity

resolution for dual frequency measurements. The effect of multipath on ionospheric measurements using GPS was presented by Bishop et al. [1985]. Some receivers have incorporated special features to reduce multipath, like narrow early-late spacing [Van Dierendonck et al., 1992]. Van Nee [1992] studied the tracking performance of the delay lock loop (DLL) and proposed a optimum GPS receiver structure in the presence of multipath.

#### 4.1 CODE AND CARRIER MULTIPATH

In GPS signals, the carrier frequencies are modulated by Pseudo Random Noise codes, either C/A-code or P-code. A simplified GPS signal can be written as:

$$S_d(t) = A_p P(t) \cos(\omega t + \Psi) \quad (4.1)$$

where  $\omega$  is the frequency of the carrier, and  $\Psi$  is the carrier initial phase. The Pseudo Random Noise code  $P(t)$  is a  $\pm 1$  pseudo-random sequence with a clock rate of 1.023 Mbps for C/A code and 10.23 Mbps for P-code.  $A_p$  is the amplitude of the Pseudo Random Noise code. The navigation message sequence is not presented here since it is of no interest.

In the presence of multipath, the GPS signal received at the antenna will consist of both the direct signal  $S_d(t)$  and its delayed replica  $S_r(t)$  due to reflection:

$$\begin{aligned} S(t) &= S_d(t) + S_r(t) \\ &= A_p P(t) \cos(\omega t + \Psi) + \alpha A_p P(t - \delta) \cos(\omega t + \Psi - \Psi_r) \end{aligned} \quad (4.2)$$

where  $\delta$  and  $\Psi_r$  are the time and phase delay of the reflected signal, and  $\alpha$  is the ratio of reflected/direct signal voltages.

In a GPS receiver, the Delay Lock Loop (DLL) is used to measure the range from the receiver antenna to the satellite. There are two kinds of widely used DLLs, namely the coherent DLL and noncoherent DLL. The structure of the noncoherent delay lock loop is shown in Figure 4.2 [Van Nee, 1992].

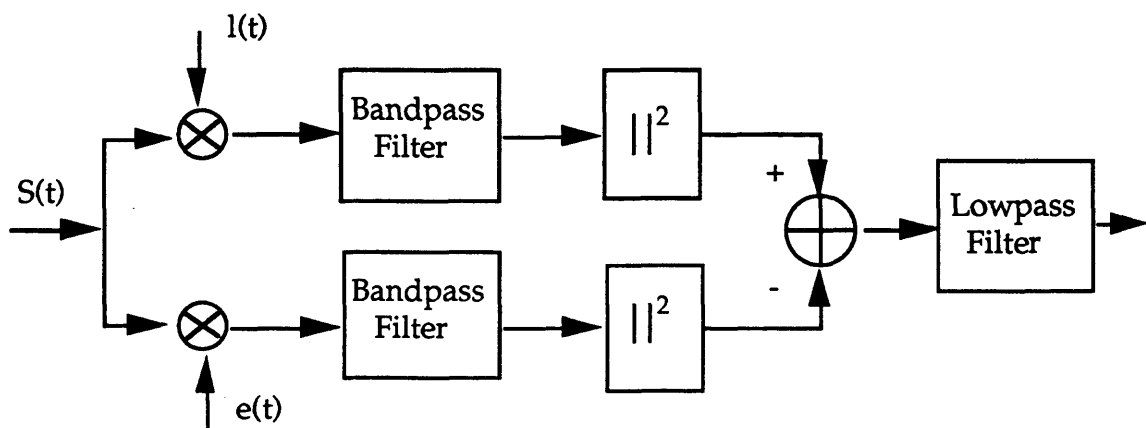


Figure 4.2 Noncoherent DLL Structure

In a noncoherent DLL, the input signal  $S(t)$  is coherently correlated with two local spread-spectrum codes with a relative spacing  $\tau_d$ , the early code  $e(t)$  and the late code  $l(t)$ . The two correlation functions are then squared in envelope detectors and subtracted to form a correction signal to drive the Voltage-Controlled-Oscillator (VCO). The VCO in turn drives the PRN generator to align the locally generated PRN code with the received code. In the coherent DLL, the envelope detectors are not used, instead the carrier tracking loop is added.

Breeuwer [1991] mathematically described the multipath error in a noncoherent delay lock loop. The formula can be written as:

$$\begin{aligned}
D(\tau) = & [R^2(\tau + \tau_d) - R^2(\tau - \tau_d)] \\
& + 2\alpha \cos \Psi_r [R(\tau + \tau_d)R(\tau + \tau_d - \delta) - R(\tau - \tau_d)R(\tau - \tau_d - \delta)] \\
& + \alpha^2 [R^2(\tau + \tau_d - \delta) - R^2(\tau - \tau_d - \delta)] = 0
\end{aligned} \tag{4.3}$$

The multipath error in a coherent DLL is given in [Bishop et al., 1985]:

$$\begin{aligned}
D(\tau) = & [R(\tau + \tau_d) - R(\tau - \tau_d)] \cos(\theta_m) \\
& + \alpha [R(\tau + \tau_d)R(\tau + \tau_d - \delta) - R(\tau - \tau_d)R(\tau - \tau_d - \delta)] \cos(\Psi_r - \theta_m) = 0
\end{aligned} \tag{4.4}$$

where

$$\theta_m = \tan^{-1} \left( \frac{\alpha R(\tau - \delta) \sin \Psi_r}{R(\tau) + R(\tau - \delta) \cos \Psi_r} \right) \tag{4.5}$$

$R(\tau)$  is the PRN cross-correlation function:

$$R(\tau) = \begin{cases} 1 - \frac{\tau}{T} & |\tau| \leq T \\ 0 & |\tau| > T \end{cases} \quad T = \text{PRN chip time} \tag{4.6}$$

$\tau_d$  is the early-late correlation spacing.

Carrier phase measurements are made on the phase lock loop (PLL). On the phase lock loop, the code and carrier are separated to enable phase to be locked and the bit information of the satellite message to be extracted. This technique is also named reconstruction of the carrier. In most cases a Costas Loop is used. In the loop, the demodulated satellite carrier phase signal is aligned with the phase signal of the receiver's oscillator. The output observable is the carrier beat phase, the relative phase between the received carrier signal and the internal reference carrier signal.

The effect of multipath on the carrier phase can be understood from the vector plot in Figure 4.3. The instantaneous carrier multipath error is the angle

$\Psi_m$  between the direct signal vector  $S_d(t)$  and the sum vector  $S(t)$  of direct and reflected signals.

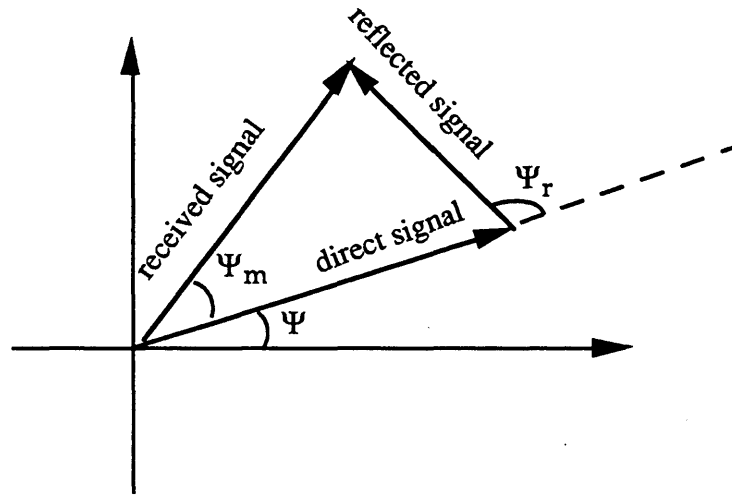


Figure 4.3 Multipath Effect on Carrier Phase

Let us assume that the Pseudo Random Noise code  $P(t)$  has been properly removed in the PLL. The received carrier signal (4.2) then becomes:

$$S(t) = A_p \cos(\omega t + \Psi) + \alpha A_p \cos(\omega t + \Psi - \Psi_r) \quad (4.7)$$

or [Georgiadou et al., 1987]:

$$S(t) = \beta A_p \cos(\omega t + \Psi + \Psi_m) \quad (4.8)$$

where  $\beta = \sqrt{1 + 2\alpha \cos \Psi_r + \alpha^2}$  is the change factor in signal voltage amplitude, and  $\Psi_m = \arctan\left(\frac{\alpha \sin \Psi_r}{1 + \alpha \cos \Psi_r}\right)$  is the multipath error in the carrier phase.

Georgiadou et al. [1987] also considered the case of multiple reflectors. In this case, the received signals are

$$S(t) = A_p \cos(\omega t + \Psi) + A_p \sum_{i=1}^M \alpha_i \cos(\omega t + \Psi - \Psi_r^i) \quad (4.9)$$

where  $M$  is the number of reflections, and  $\alpha_i$  and  $\Psi_r^i$  denote the amplitude and the phase delay of the  $i$ th reflected signal, respectively. The total voltage amplitude and the multipath induced carrier phase error are given by [Georgiadou et al., 1987]:

$$\beta = \left[ \left( 1 + \sum_{i=1}^M \alpha_i \cos \Psi_r^i \right)^2 + \left( \sum_{i=1}^M \alpha_i \sin \Psi_r^i \right)^2 \right]^{1/2} \quad (4.10)$$

$$\Psi_m = \arctan \left( \frac{\sum_{i=1}^M \alpha_i \sin \Psi_r^i}{1 + \sum_{i=1}^M \alpha_i \cos \Psi_r^i} \right), \quad (4.11)$$

Equation (4.11) can be approximated by:

$$\Psi_m = \frac{1}{2\pi} \sum_{i=1}^M \alpha_i \sin \Psi_r^i \quad (\text{in cycles}) \quad (4.12)$$

As we already know, due to the changing geometry between satellite, reflector and antennas, the phase difference  $\Psi_r^i$  between direct and reflected signals will slowly vary in time, resulting in periodic variations of the carrier phase multipath. From Figure 4.3 we can see that when the reflected signal and the received signal are perpendicular, the multipath error in carrier phase reaches its maximum so that:

$$\Psi_{\max} = \pm \arcsin \alpha \quad (4.13)$$

The maximum multipath error in carrier phase depends only on the relative signal strength of the reflected signal expressed by the factor  $\alpha$ . In the worst case where  $\alpha = 1$ , this maximum value is  $\Psi_{\max} = 90^\circ$ , which is equivalent to a range error of about 4.8 cm for L1 signal and 6.0 cm for L2 signal.

## 4.2 MULTIPATH DETECTION AND REDUCTION

A major problem in the study of multipath is the isolation of its effects on actual pseudorange and carrier phase measurements. Since the early stages of GPS development, a number of approaches have been investigated to determine the multipath errors on both pseudorange and carrier phase measurements.

### 4.2.1 Code Multipath Detection

The simplest method to determine multipath error in pseudorange measurements is to compare the differences between pseudorange and carrier phase measurements [Evans, 1986]. The pseudorange is obtained by multiplying propagation time from satellite to receiver by the propagation velocity of the GPS signal. Pseudorange measurements are influenced by a number of error sources. The carrier phase contains the same information and error sources as the pseudorange except for the ionospheric effect. The ionosphere advances the carrier phase and delays the pseudorange. So a correction for the ionospheric effect has to be made.

Since the range information contained in the pseudorange and carrier phase is highly correlated, when we subtract the carrier range measurements from the pseudorange measurements we are eliminating the geometric information. Systematic errors such as orbit, receiver clock and tropospheric errors will be canceled out as they have similar effects on the pseudorange and carrier phase. Since the multipath error on carrier phase measurements is two orders of magnitudes smaller than that on pseudorange measurements, this leaves for the most part, pseudo-range multipath, receiver measurement noise and a constant bias caused by the unsolved cycle ambiguity from the carrier phase.

To demonstrate the multipath error in pseudorange measurements, the data sets collected with NovAtel GPSCard™ receivers at Fort Belvoir area [Lachapelle et al., 1993] were analysed. The code and carrier measurements were first corrected for the relative effect of the ionosphere, and then differenced. Since GPSCard™ is a single-frequency receiver, it is impossible to calculate the ionospheric delay by dual frequency data. A second order polynomial is used instead to subtract the long term bias. The cycle ambiguity was removed with an accuracy of several cycles by subtracting the initial code/carrier bias, and the carrier phase cycle slips were detected and corrected so that the ambiguity bias was constant throughout the data span. The above difference can, therefore, be assumed to consist mostly of code noise and multipath. Figure 4.4 shows the range differences for SV3 on day 342. From the figure, it can be seen that even though a narrow spacing correlation technique is used in the receiver, the multipath error can still reach up to three metres.

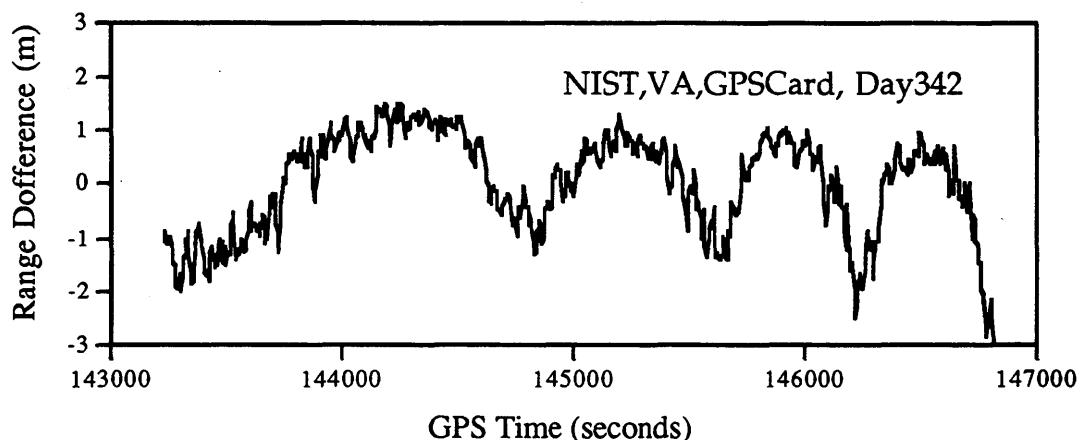
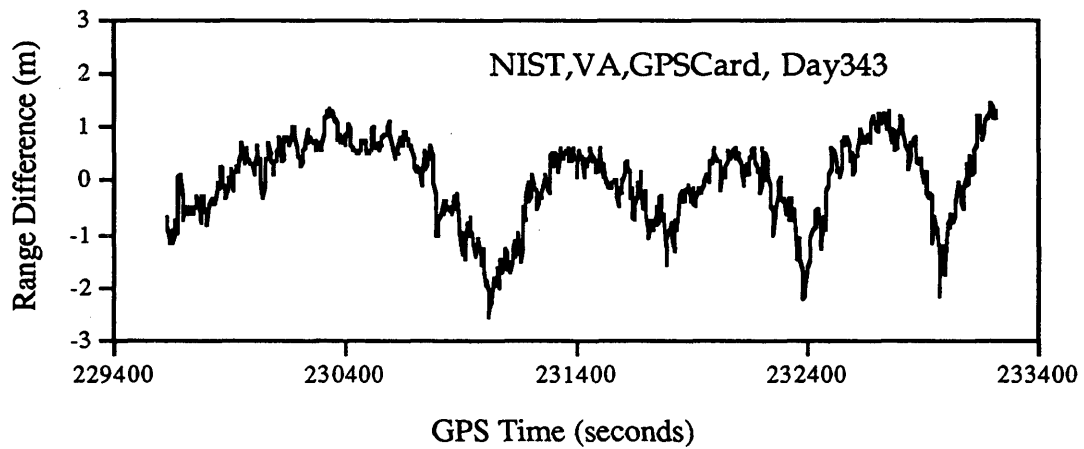


Figure 4.4 Code Multipath Error on Day342



**Figure 4.5 Code Multipath Error on Day343**

Multipath errors in the pseudorange measurements collected over two consecutive days will be highly correlated when the surrounding conditions stay exactly the same. Figure 4.5 shows the range differences for the same satellite on the second day at the same place. To demonstrate the repeated day-to-day multipath effects, the cross-correlation function is determined for two days of range differences and is shown in Figure 4.6. The cross-correlation function is defined as the standard cross correlation divided by the standard deviation of each data set. This normalizes its value to be between -1 and +1. Let

$$X_1(i), \quad i = 0, 1, 2, \dots, N \quad \{\sigma_{X_1}\} \quad (4.14)$$

$$X_2(i), \quad i = 0, 1, 2, \dots, N \quad \{\sigma_{X_2}\} \quad (4.15)$$

be time series representing the pseudorange differences on the first and second day,  $i$  is the epoch and  $\sigma_{X_1}, \sigma_{X_2}$  the standard deviation of  $X_1(i)$  and  $X_2(i)$ , respectively. The normalized correlation function  $r(k)$  is:

$$r(k) = \frac{\sum_{i=0}^{N-k-1} x_1(i) \cdot x_2(i+k)}{\sigma_{X_1} \sigma_{X_2} (N-k)} \quad (4.16)$$

A peak (0.711) can be seen in Figure 4.6 at 240 seconds delay. This is the multipath signature since the satellite orbit repeats itself approximately 4 minutes earlier each day.

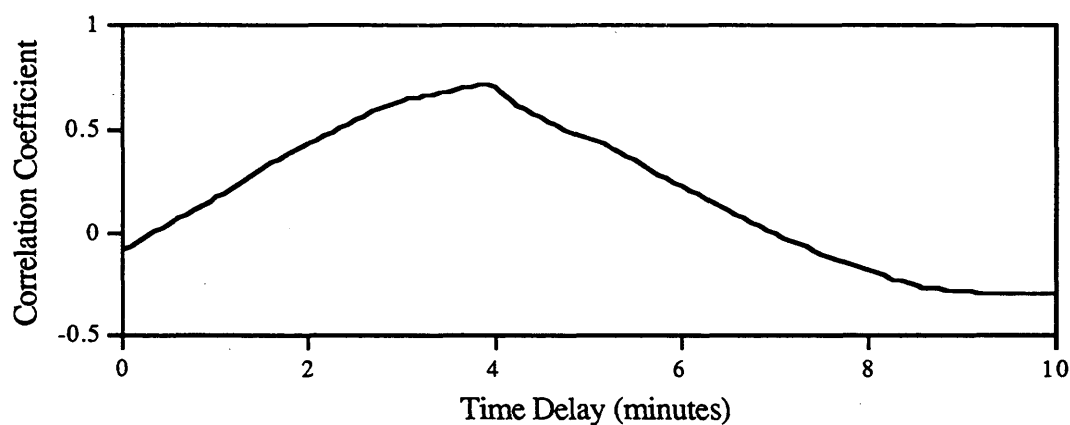


**Figure 4.6 Cross-correlation Function of Multipath**

#### 4.2.2 Carrier Phase Multipath Detection

In GPS carrier phase measurements, the multipath error  $\Psi_m$  is indistinguishable from a change of the true phase of the direct signal. Only the analysis of adjustment residuals could reveal suspicious systematic variations. However, dual frequency carrier phase observations can make it possible to detect the occurrence of multipath directly in the measurement records, at least on short baselines [Georgiadou and Kleusberg, 1987].

The main purpose of using dual frequency carrier phase measurements for geodetic applications is to eliminate the dispersive ionospheric delay. For short baselines, the actual differential ionospheric delay will be very small as the behavior of the ionosphere does not frequently show short periodic variations, so periodic variation in the differential ionospheric delay as computed from dual frequency carrier phase measurements will be an indicator of multipath contamination.

With a dual frequency receiver, observation equations can be formed for L1 and L2 carrier signals [Lachapelle, 1992d]:

$$\Phi_{L1} = \rho + d\rho + c(dt - dT) + \lambda_1 N_1 - d_{ion1} + d_{trop} + \lambda_1 \Psi_m^1 + \varepsilon(L1) \quad (4.17)$$

$$\Phi_{L2} = \rho + d\rho + c(dt - dT) + \lambda_2 N_2 - d_{ion2} + d_{trop} + \lambda_2 \Psi_m^2 + \varepsilon(L2) \quad (4.18)$$

where

$\Phi_{L1}, \Phi_{L2}$  are the carrier phase measurements on L1 and L2,

$\Psi_m^1, \Psi_m^2$  are the carrier phase multipath errors on L1 and L2.

After differencing between the two frequencies, we obtain:

$$\begin{aligned} d\Phi &= \Phi_{L1} - \Phi_{L2} \\ &= (d_{ion1} - d_{ion2}) + (\lambda_1 N_1 - \lambda_2 N_2) + (\lambda_1 \Psi_m^1 - \lambda_2 \Psi_m^2) + \varepsilon(L1, L2) \end{aligned} \quad (4.19)$$

The only effects remaining after inter-frequency differencing of the carrier phase observations are the dispersive ionospheric delay, the initial inter-frequency ambiguities, the carrier phase multipath errors, and measurement noise. The initial inter-frequency ambiguities will remain constant as long as the carrier phase data are cycle slip free. The carrier phase multipath error is indistinguishable from the ionospheric delay for a single station. However, for a

short baseline only a few kilometres in length, the differential ionospheric delay between two stations will be very small. The difference of inter-frequency differences between two stations may indicate the presence of carrier phase multipath error at both sites:

$$\begin{aligned} DD = d\Phi_M - d\Phi_R = & (d_{ion1} - d_{ion2})_M - (d_{ion1} - d_{ion2})_R \\ & + (\lambda_1 N_1 - \lambda_2 N_2)_M - (\lambda_1 N_1 - \lambda_2 N_2)_R \\ & + (\lambda_1 \Psi_m^1 - \lambda_2 \Psi_m^2)_M - (\lambda_1 \Psi_m^1 - \lambda_2 \Psi_m^2)_R \\ & + \varepsilon(L1, L2, M, R) \end{aligned} \quad (4.20)$$

Assuming the actual differential ionospheric delay is zero for short baselines, equation (4.20) can be written as:

$$DD = (\lambda_1 \Psi_m^1 - \lambda_2 \Psi_m^2)_M - (\lambda_1 \Psi_m^1 - \lambda_2 \Psi_m^2)_R + \text{constant} + \text{white noise} \quad (4.21)$$

where  $( )_M$  and  $( )_R$  indicate that the quantities in brackets are calculated at the monitor and remote stations, respectively.

Equation (4.21) represents a superposition of multipath errors on both frequencies and at both sites. Applying the carrier phase multipath error model (4.12) in equation (4.21) and recognizing that there are multiple simultaneous reflections, we obtain:

$$DD = \sum_{i=1}^M \frac{\alpha_i}{2\pi} (\lambda_1 \sin \Psi_r^{1i} - \lambda_2 \sin k \Psi_r^{2i}) + C \quad (4.22)$$

where  $i$  denotes the  $i$ -th reflected signal. The summation indicated by  $\Sigma$  is to be extended over all reflected signals at both monitor and remote stations.  $k$  is the ratio of the wavelengths between L2 and L1.

An experiment at The University of Calgary was conducted to investigate the carrier phase multipath error. To avoid any errors resulting from differential atmospheric delays and inaccurately known satellite orbits, a very short baseline on the upper part roof (F Block) of the Engineering Building was selected for the test. The proximity of several ventilation shafts with convex reflective metallic surfaces ensures this location to be a relatively high multipath environment. Two Ashtech P-XII receivers were used to observe the 7m baseline. The inter-frequency differences for SV03 were computed at both sites according to equation (4.19). The time series so obtained were then reduced to differential ionospheric delay using equation (4.21).

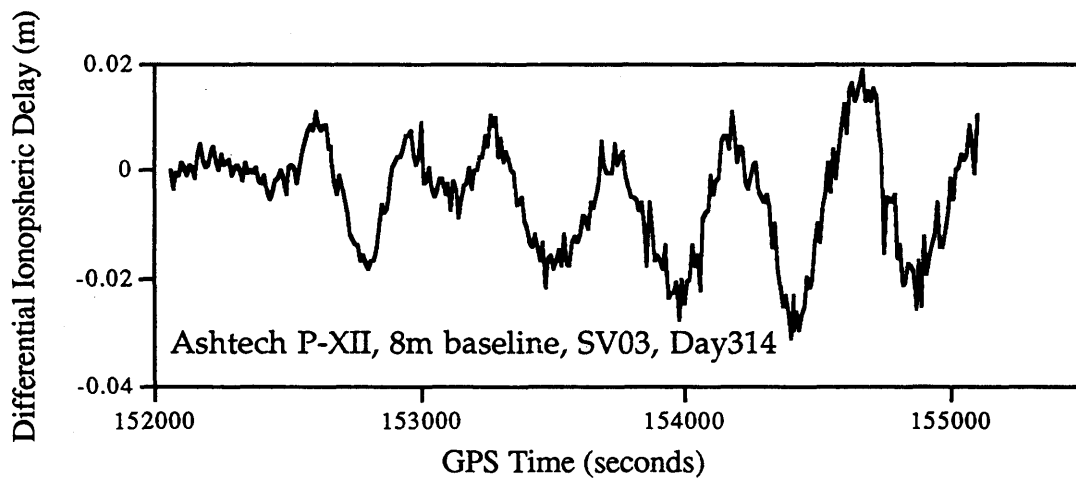


**Figure 4.7 Differential Ionospheric Delay for SV03 on Day314 (Carrier Phase)**

The results on day 314 are shown in Figure 4.7. The observation was repeated the next day in order to assess the correlation of the differential ionospheric delays. The differential ionospheric delays on day 315 are shown in Figure 4.8. The correlation coefficients of the differential ionospheric delays between the two consecutive days are shown in Figure 4.9. The high correlation at 4 minutes

clearly indicates that the variations shown in Figures 4.7 and 4.8 are related to repeated satellite geometry, and therefore must be attributed to multipath. The rather regular periodic pattern in these figures indicate that multipath could originate from planar reflectors. However, due to the multitude of conducting material in the surroundings of the observation site, the unambiguous identification of a particular reflector was not possible.

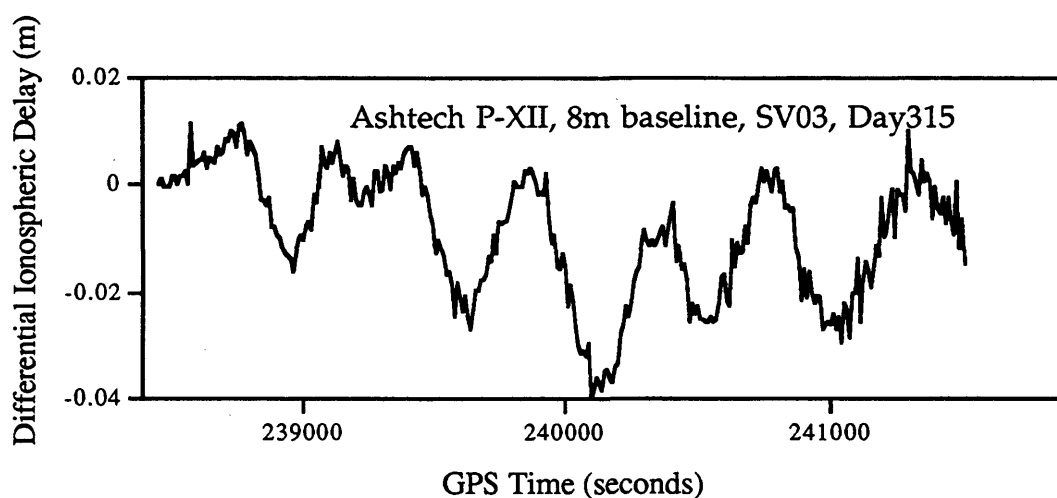


**Figure 4.8 Differential Ionospheric Delay for SV03 on Day315 (Carrier Phase)**

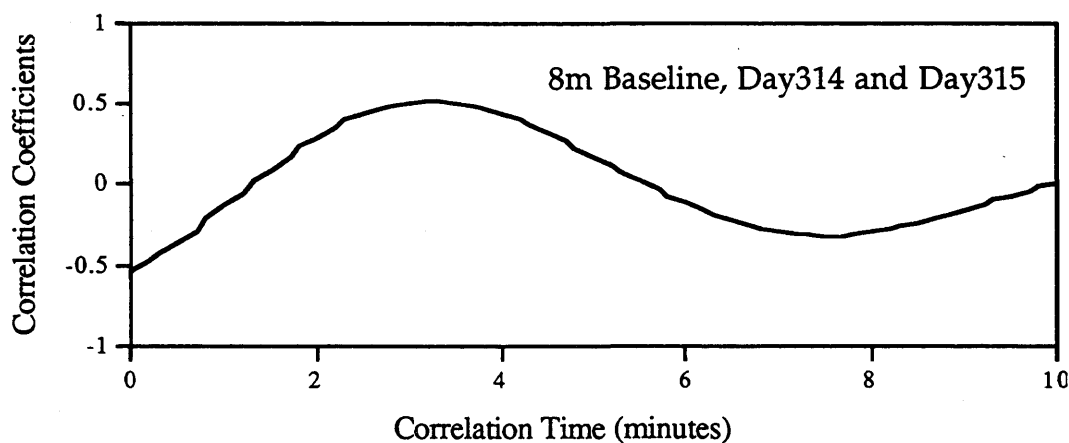


**Figure 4.9 Correlation of Differential Ionospheric Delays between Day 314 and Day 315**

### 4.2.3 Multipath Error Reduction

Multipath errors affect not only the accuracy of the position, but also the site occupation time to resolve the carrier phase ambiguities. It is hence important to avoid multipath. Possible measures to minimize the effect are:

(1) Improve the receiver performance. The narrow Early-Late (E/L) correlation spacing technique used in NovAtel GPSCard™ receiver reduces the multipath error and noise level in pseudorange measurements [Van Dierendonck et al., 1992]. However, the multipath errors in carrier phase measurements are not reduced. Meehan and Young [1992] described several techniques to reduce the code and carrier multipath developed at the Jet Propulsion Laboratory (JPL). Some of them have been tested with the Turbo Rogue GPS receiver.

(2) Mitigate the multipath error in code and carrier phase measurements with mathematical models. Cohen et al. [1991] used a spherical harmonic function of satellite elevation and azimuth to represent the multipath error. Another approach is to consider the multipath error as a random process. In this case multipath can be reduced by using stochastic filters [Van Graas et al., 1991].

(3) Select an antenna site distant from reflecting objects, and design antenna/backplane combinations to further isolate the antenna from its surroundings, such as the use of choking ground plane and RF absorbing material.

To assess the effectiveness of reducing multipath with the use of choking and RF ground plane, six days of data were collected for three cases, namely (1)

no extended ground plane, (2) use of RF absorbent ground plane, and (3) use of a chokering. The data was collected by one Ashtech P-XII receiver on two consecutive days for each of these cases. The same observation span was used for the two days in order to assess the correlation in pseudorange measurements. The antenna was placed on The University of Calgary's Engineering roof, where large multipath errors have been observed [Lachapelle et al., 1989].

The RF absorbent ground plane, which was provided by the Department of Electrical Engineering, The University of New Brunswick, was made of carbon impregnated foam, had a dimension of 1.5 m  $\times$  1.5 m, and was in the shape of an inverted cone to shield signals coming from an elevation angle  $<15^\circ$ . The chokering groundplane manufactured by EM Technologies in Fredericton for the Ashtech P-XII antenna was made of aluminum and had a diameter of 37 cm.

The pseudorange differences were calculated for each day using the approach discussed in section 4.2.1. The code or pseudorange multipath can now be isolated from the code noise if one assumes that the pseudorange differences contain only measurement noise and multipath. The rms of the pseudorange difference  $\sigma_t$  can be written as

$$\sigma_t^2 = \sigma_{\text{noise}}^2 + \sigma_{\text{mult}}^2 \quad (4.23)$$

The noise  $\sigma_{\text{noise}}$  was estimated through zero-baseline analysis as 1.5m for C/A-code and 20 cm for P-code.  $\sigma_{\text{mult}}$  can then be calculated using equation (4.22). Table 4.1 summarizes the results for the three test cases for SV11.

A first analysis of Table 4.1 can be made by determining the consistency between the results achieved on each day. For each test, there is a very high

correlation between the standard deviations of each day. For example, the 'RF ground plane' case gives standard deviations of 1.81 m, 0.27 m, and 0.33 m for the C/A, P-L1 and P-L2 data, respectively, on March 6, while the data for March 7 gives corresponding standard deviations of 1.69 m, 0.25 m, and 0.23 m.

**Table 4.1 Multipath Analysis of ASHTECH P-XII for Satellite 11**

Case	Date	Obs	RMS	STD $\sigma_t$	$\sigma_{mult}$
No extended ground plane	Mar 11	C/A	2.47	1.92	1.20
		P (L1)	0.41	0.30	0.22
		P (L2)	1.15	0.55	0.51
	Mar 12	C/A	2.71	2.36	1.82
		P (L1)	0.87	0.33	0.26
		P (L2)	1.25	0.53	0.49
RF Ground plane	Mar 6	C/A	2.48	1.81	1.01
		P (L1)	0.67	0.27	0.18
		P (L2)	0.30	0.23	0.11
	Mar 7	C/A	3.26	1.69	0.78
		P (L1)	0.25	0.25	0.15
		P (L2)	0.49	0.23	0.11
Choke ring	Mar 14	C/A	1.86	1.84	1.07
		P (L1)	0.29	0.23	0.11
		P (L2)	0.65	0.15	0.00
	Mar 15	C/A	2.15	1.96	1.26
		P (L1)	0.16	0.16	0.00
		P (L2)	0.18	0.17	0.00

The rms code multipath effect is shown in the last column of Table 4.1. The results show that the C/A(L1) multipath is larger for the case when no extended groundplane is used, i.e. 1.20 m and 1.82 m for March 11 and 12, respectively, compared to the case when a chokering or RF absorbent ground plane is used

(generally 1 m). For P-L1 and P-L2, the noise is significantly smaller than C/A(L1) noise, as expected. The magnitude is larger when no extended ground plane is used. The results also show that in this case, the choke ring is an effective method to minimize code multipath whether C/A code or P code data are collected. No significant multipath effect on P-L2 is apparent on March 14, and on P-L1 and P-L2 on March 15. Although this is theoretically possible, the data has to be interpreted with caution at this time due to the various biases and other problems affecting the Ashtech P-XII receiver.

### 4.3. MULTIPATH EFFECT ON RAPID STATIC DGPS

Although various measures can be taken to reduce the multipath error in code and carrier phase measurements, multipath error contamination is still inevitable in many cases. For a short baseline, multipath errors can dominate the adjusted residuals and thus affect the site occupation time needed to resolve the ambiguities. One approach to investigate the multipath effect on the required time to resolve integer carrier phase ambiguities is to analyse the spectrum of the carrier phase multipath.

Equation (4.12) can be rewritten in the form of a Fourier series:

$$\Psi_m = \sum_{i=0}^{\infty} [A_i \cos(2\pi f_i t) + B_i \sin(2\pi f_i t)] \quad (4.24)$$

where  $A_i$ ,  $B_i$  are the amplitudes of the carrier phase multipath error at frequency  $f_i$ . The power spectrum  $P_i$  is defined by:

$$P_i = \sqrt{(A_i^2 + B_i^2)} \quad (4.25)$$

By analyzing the power spectrum of the carrier phase multipath errors, the major multipath frequencies can be identified. As a rule-of-thumb, the observation time should be as long as the largest multipath period to average out its effects, provided that the satellite geometry is optimal.

As an example, the 519 m baseline data set described in section 3.2.1 has been analysed. Variance-covariance analysis of the carrier phase ambiguities indicated that 250 seconds of observation was enough to isolate the ambiguities. However, the success rate of trials to resolve the integer ambiguities using 250 seconds of observation time was 50% due to strong multipath. Table 4.2 shows the major multipath periods calculated by the Fourier analysis.

Using the information from Table 4.2, the longest multipath periods for the 519m baseline were found to be about 450 seconds. Using 450 seconds of observation time for the baseline in rapid static mode, nine out of ten trials were successful in resolving the integer ambiguities, as shown in Table 4.3. For the purpose of comparison, the success rate of trials using 350 seconds (< multipath periods) are also listed in Table 4.3. From this table it can be seen that when the site occupation time is less than the major multipath period, the success rate in resolving the integer ambiguities is significantly lower.

To assess whether the averaging of multipath is indeed a necessary condition for integer ambiguity resolution over short baselines, the differences between the estimated float ambiguities and the true integer ambiguities are plotted against the observation time in Figure 4.10. From this figure we can see that, due to strong multipath errors in carrier phase measurements, the estimated float ambiguities become stable only after 400 seconds of observation time. Hence 450

seconds of observation time is really needed to isolate the ambiguities in this case. This conclusion is also true for long baselines to obtain a more accurate baseline determination using a float solution.

**Table 4.2 Major Multipath Periods in 519m Baseline.**

Satellite	Major Periods
3	449.0 seconds
16	383.0
17	520.0*
21	290.0
23	324.0
26	179.0

\* Small magnitude

**Table 4.3 Success Rate of Trials Using Different Observation Time**

Occupation Time	Success Rate
450 seconds	90%
350 seconds	50%

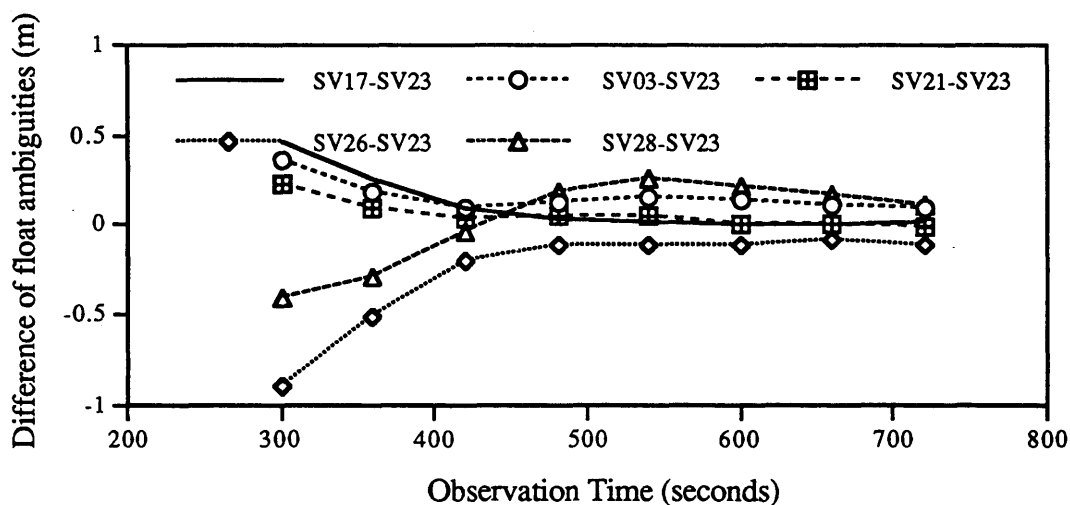


**Figure 4.10 Accuracies of Float Ambiguity Estimation**

The main problem with the power spectrum analysis in estimating the major multipath periods is that we cannot obtain the carrier phase multipath errors in real-time. For single-frequency receivers, the carrier phase multipath error will not be obtained until the ambiguities are successfully resolved and the carrier phase residuals are calculated.

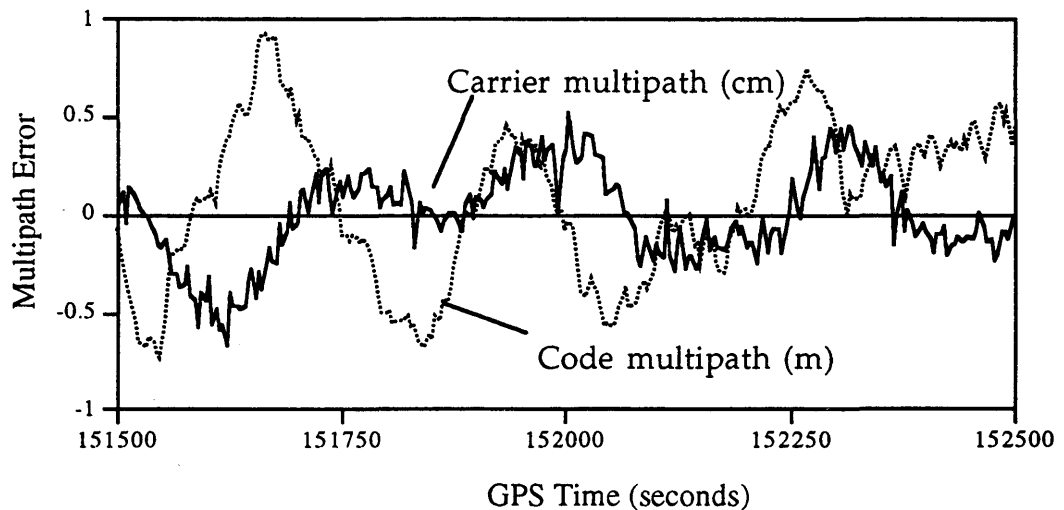


**Figure 4.11 Code and Carrier Multipath**

Fortunately, as Breeuwer [1991] pointed out, the multipath error in carrier phase measurements has the same frequency as the multipath error in pseudorange measurements. The relation between the multipath error on pseudorange and that on carrier phase measurements for SV26 of the 519m baseline is illustrated in Figure 4.11. Multipath errors on other satellites of this baseline have the same relation although the pattern is not so clear. This figure shows that the carrier multipath is generally minimal when the code multipath is maximal and vice versa. Hence it is only necessary to calculate the multipath error in pseudorange measurements in real-time in order to obtain the major periods of the carrier phase multipath errors.

## CHAPTER 5

### IONOSPHERIC EFFECT MODELING FOR SINGLE FREQUENCY USERS

The ionospheric propagation delay is a major source of concern to GPS users since it can reach an extreme value of 50 m at times of high solar activity [Wells et al., 1987]. Four methods can be used to eliminate or reduce the the ionospheric range errors for precise positioning applications:

(1) Differencing observations from one satellite between two stations to reduce the ionospheric effect, based on the assumption that the ionospheric delay is, to some extent, spatially correlated between the receivers.

(2) Taking measurements on L1 and L2 and using the dispersive nature of the ionosphere to eliminate the first order propagation delay term.

(3) Predicting the delay using an ionospheric model. A simplified model is transmitted as part of the satellite navigation message. This model can generally compensate 50% to 75% (rms) of the ionospheric effect at mid-latitude [Klobuchar, 1987].

(4) If only L1 code and carrier phase measurements are available, use the code-carrier phase divergence property to predict the ionospheric group delay (and carrier phase advance since the latter is identical to the former with the opposite sign). This however entails the availability of relatively precise L1 code

measurements largely free of multipath errors. The use of divergence measurements yields the relative ionospheric delay since the initial observation epoch. Appropriate modeling can also yield the initial absolute delay, although with a lower level of accuracy (Cohen et al., 1992). While it is recognized that the relative ionospheric delay is sufficient for static differential GPS, the absolute delay is needed for many other single point and differential static and kinematic applications.

In this chapter, the latter method is investigated using successively P(L1) measurements and precise C/A code measurements obtained with a narrow correlator spacing L1 C/A code receiver [Qiu et al., 1993]. Two important characteristics of the latter receiver type are a 10-cm receiver code noise level, as opposed to the 1 - 3 m level which typifies wide correlator C/A code receivers, and increased resistance to code multipath [Cannon and Lachapelle, 1992; Van Dierendonck et al., 1992]. First, the methodology used to derive not only the relative ionospheric delay over time but also the absolute delay, is described.

## 5.1 THE IONOSPHERE AND GPS SIGNAL PROPAGATION

The ionosphere is that region of the earth's atmosphere in which ionizing radiation (principally from ultraviolet and x-ray emissions) causes electrons to exist in sufficient quantities to affect the propagation of radio waves [Langley, 1992]. The dimension of this layer of ionized material vary both spatially and temporally, but general guidelines are 50 -60 km and 1000 km for the lower and upper limits respectively. To be exact, the ionized part of the atmosphere extends to interplanetary space and merges with the plasma although the electron density ( the number of electrons per cubic metre) decreases significantly above

800 km. What we observe is the combined effect from the ionosphere and the plasmasphere, because the GPS orbits are located far above the ionospheric layer. However, an observer on the surface of the earth, who uses GPS as a tool for positioning or navigation, has no need to separate the ionospheric and the plasmaspheric effect. In this thesis, as in most literature, the term ionospheric delay is therefore understood as the combined effect.

The ionosphere is composed of free electrons. These charged particles are influenced by solar activity and the geomagnetic field. The spatial distribution of electrons and ions is mainly determined by two processes in the ionosphere:

(1) Photo-chemical processes; they depend on the insolation of the sun, and they govern the production and decomposition rate of the ionized particles.

(2) Transportation processes; they cause motion of the ionized layers.

Both processes create different layers of ionized gas at different altitudes. The main layers are known as the D-, E-, F<sub>1</sub>-, and F<sub>2</sub>- layer [Seeber, 1993].

The state of the ionosphere is described by the electron density  $n_e$  with the unit of number of electrons per m<sup>3</sup>. When radio waves, such as those from a GPS satellite, pass through the ionosphere, they travel in curved paths and experience a delay. This is caused by electromagnetic interactions between the electrically charged field of the ionosphere and the external field of the penetrating wave.

The impact of the curved path on the code and phase measurements are very small. Applying the empirical formula given by Brunner and Gu [1991], the residual range error, which is the difference between the dual-frequency corrected range and the true range, due to bending alone, is estimated to be

about 4 mm at a 10° elevation angle and less than a millimetre for elevations above 30°. The bending effect will be ignored in the following analysis; the two signals will be assumed to travel along the same straight path.

The impact of the ionosphere on the signal propagation delay in the radio frequency domain is mainly characterized by dispersion. The refraction index describing the propagation of phase can be written as a power series:

$$n_p = 1 + \frac{c_2}{f^2} + \frac{c_3}{f^3} + \dots \quad (5.1)$$

The coefficients  $c_i$  are independent of the carrier frequency. However, through the electron density  $n_e$ , they depend on the state of the ionosphere. The coefficient  $c_2$  is estimated to be  $c_2 = -40.3n_e$ , hence we find the approximate relation:

$$n_p = 1 - \frac{40.3n_e}{f^2} \quad (5.2)$$

The refraction index  $n_g$  of the group delay is related to  $n_p$  by [Seeber, 1993]:

$$n_g = n_p + f \frac{dn}{df} \quad (5.3)$$

With (5.1), it follows from (5.3) that

$$n_g = 1 - \frac{c_2}{f^2} - \frac{2c_3}{f^3} - \dots \quad (5.4)$$

Truncating after the first order term, it follows that

$$n_g = 1 + \frac{40.3n_e}{f^2} \quad (5.5)$$

GPS phase measurements are dependent upon the phase refraction index  $n_p$ . The ionospheric phase delay  $\delta\Phi_{ion}$  is [Wells et al., 1987]:

$$\delta\Phi_{ion} = \int_R^S (n_p - 1) ds = -\frac{40.3}{f^2} \int_R^S n_e ds = -40.3 \frac{N_T}{f^2} \quad (5.6)$$

where  $N_T$  is the Total Electron Content (TEC), counted along the signal path  $s$  between the satellite  $S$  and the receiver  $R$ . The code measurements, on the other hand, are governed by the refraction index of group velocity  $n_g$ . The ionospheric group delay  $\delta P_{ion}$  is:

$$\delta P_{ion} = \int_R^S (n_g - 1) ds = 40.3 \frac{N_T}{f^2} \quad (5.7)$$

A comparison of (5.6) with (5.7) makes it clear that the effect of the ionosphere on the phase and the group velocity is approximately equal in magnitude, but has an opposite sign with each.

Because of the approximation in equations (5.2) and (5.5), equations (5.6) and (5.7) are called the first order ionospheric refraction correction. The remaining model errors reach only a few centimetres. Table 5.1 shows the maximum range errors that can be expected for both GPS frequencies, and for the dual-frequency corrected signal, both in vertical direction [Bassiri and Hajj, 1993].

**Table 5.1 Maximum Vertical Ionospheric Range Error  
[Bassiri and Hajj, 1993].**

	L1	L2	L1/L2
1 <sup>st</sup> order: $1/f^2$ term	16.2 m	26.7 m	0.0 m
2 <sup>nd</sup> order: $1/f^3$ term	1.6 cm	3.3 cm	1.1 cm
3 <sup>rd</sup> order: $1/f^4$ term	0.9 mm	2.4 mm	0.7 mm

## 5.2 IONOSPHERIC EFFECT ON BASELINE DETERMINATION

The ionosphere is a dispersive medium. The ionospheric effect is frequency dependent. L1 and L2 phase measurements can be used to estimate the relative effect when dual-frequency measurements are available:

$$d\Phi_{\text{ion}}^{L1} = \frac{-f_2^2}{(f_1^2 - f_2^2)} \{[\Phi_{L1} - f_1 / f_2 \Phi_{L2}] - [N_{L1} - f_1 / f_2 N_{L2}]\} \quad (5.8)$$

where  $N_{L1}$  and  $N_{L2}$  are the respective ambiguity terms. Combining observations on L1 and L2 yields the ionospheric free linear combination:

$$\Phi_{L1/L2} = \frac{f_1^2}{f_2^2 - f_1^2} \Phi_{L1} - \frac{f_2^2}{f_1^2 - f_2^2} \Phi_{L2} \quad (5.9)$$

For single-frequency receivers, when simultaneously observing GPS satellites from two or more stations, the expected high degree of correlation between the ionospheric effects affecting the observations at both sites should result in the cancellation of the ionospheric error through differencing. It is under this assumption that inter-station differences of single frequency observations reduce ionospheric effects. However, as the distance between stations increases, the ionospheric effects will be less correlated. Residual ionospheric effects will remain in the carrier phase time series after inter-station differencing, and will affect the accuracy of baseline coordinate estimation.

In order to investigate the effect of the ionosphere on baseline solutions, the Ottawa GPS network data set was analyzed. The network consists of eight stations. Baseline lengths vary from 2 km to 150 km. The approximate positions of the network stations are shown in Figure 5.1. All the eight stations were observed simultaneously with Ashtech P-XII receivers on September 4, 1992.

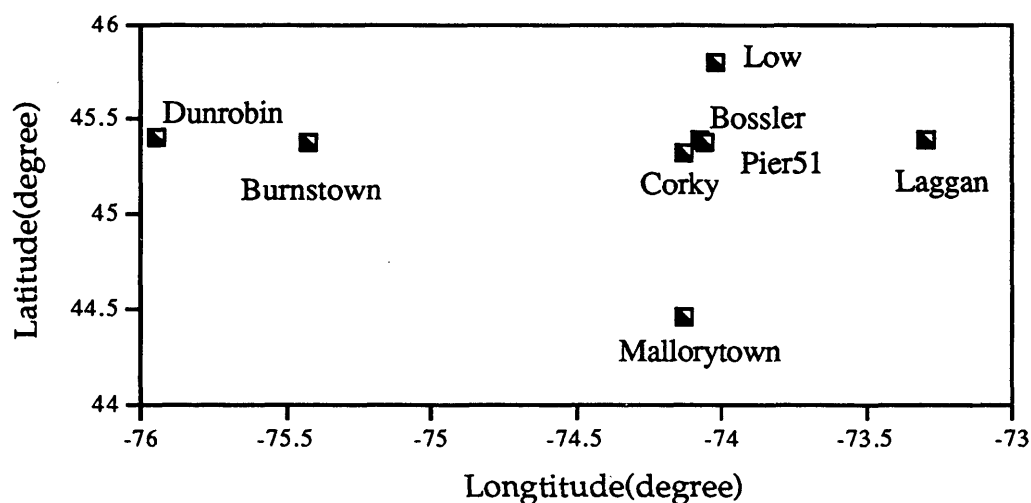


**Figure 5.1 Approximate Positions of Ottawa GPS  
Network Stations**

**Table 5.2 Ionospheric Effect on Baseline Solution**

Baseline Length(km)	Differences between solutions with and without ionospheric correction				
	$D\chi$ (cm)	$D\gamma$ (cm)	$Dz$ (cm)	3D Error (cm)	Relative Error(ppm)
2.23	0.3	0.7	1.0	1.3	5.80
10.14	0.8	0.9	1.0	1.6	1.57
45.30	2.4	2.0	1.8	3.6	0.79
50.95	5.2	2.4	5.1	7.8	1.53
95.52	2.4	4.0	0.2	4.7	0.49
103.07	8.7	0.0	19.5	21.4	2.07
105.62	5.8	10.2	6.6	13.5	1.28
109.82	12.2	3.9	13.1	18.3	1.67
137.39	6.1	25.7	6.0	27.1	2.04
146.45	12.4	6.3	9.3	16.7	1.14

The baselines in the network were processed using double difference carrier phase observations with float ambiguities. Each baseline was processed using

two different observables; i) L1 only double differences, and ii) ionospheric free L1/L2 double differences. Since no ground truth is available for this network, the solutions using ionospheric free L1/L2 double difference carrier phase observations were considered true for the purpose of comparing the results obtained with L1 only double difference carrier phase observations which are affected by the ionosphere. Table 5.2 summarizes the results.

From this table we can find that, using the L1 only double difference carrier phase solution, the large residual ionospheric errors lead to degraded positioning accuracies. As the baseline length increases beyond 100 km, the relative baseline coordinates differ from the ionospheric free solution by up to 27 cm. This level of precision might not be acceptable for certain GPS surveys. Thus the assumption of ionospheric error cancellation by differencing single frequency observations between stations does not hold under high ionospheric activity or for long inter-station distances. Early Reports [Beutler et al., 1988] have indicated that the ionospheric effects could cause problems on baselines as short as 3 kilometres. It is suggested that for baselines longer than 20 km, the ionospheric effect should be taken into account in order to achieve acceptable baseline accuracies.

It is also very interesting to investigate the effect of the dual-frequency ionospheric correction on rapid static surveying for very short baselines. It is well known that applying the dual-frequency ionospheric correction increases the noise of the ionospheric free data. Therefore, the benefit of applying the ionospheric correction for very short baselines must be weighted against the increase in measurement noise. Due to this reason, dual-frequency ionospheric corrections are generally not applied to baselines less than 10 km.

Table 5.3 shows the results of the rapid static tests for the 442 m baseline discussed in Chapter 3 with and without the ionospheric correction. Fourteen trials each using 250 seconds of data were used to determine the differences between the L1 only and the ionospheric free L1/L2 data. For the L1 only case, the correct integer ambiguities were achieved in 12 out of 14 trials. When ionospheric corrections are applied, only 6 correct integer ambiguity solutions are obtained. From the table, it can be seen that the variance ratios are always larger for the L1 only case. These results mean that the correct integer ambiguities are determined with a higher level of certainty when no ionospheric correction is applied.

**Table 5.3 Rapid Static Tests with and without Dual Frequency Ionospheric Corrections Applied (500 m Baseline)**

Trial	Ion Correction		No Ion Correction		RDOP
	Ratio	RMS (mm)	Ratio	RMS (mm)	
1	1.404*	36.3	6.401	1.4	0.321
2	2.060	2.8	34.424	1.2	0.305
3	5.423	5.3	20.053	2.0	0.290
4	5.431	3.3	43.455	1.3	0.276
5	2.995	7.3	21.066	1.1	0.258
6	3.347	2.9	27.933	0.8	0.295
7	2.276	2.6	22.202	0.7	0.309
8	1.274*	2.5	5.376	1.1	0.313
9	1.228*	2.5	6.730	1.6	0.311
10	1.001*	3.8	1.189*	1.0	0.340
11	1.006*	25.5	1.129*	4.1	0.986
12	1.346*	5.0	8.043	1.8	0.257
13	1.039*	20.3	10.530	1.8	0.260
14	1.107*	4.8	8.345	1.7	0.276

\* Ratio < 2, integer ambiguities are assumed not reliably determined.

## 5.3 IONOSPHERIC EFFECT MODELING FOR SINGLE-FREQUENCY USERS

### 5.3.1 Ionospheric Effect Modeling Using Code and Phase Measurements

If only single-frequency receivers are available, the use of equation (5.11) is impossible. An attempt can then be made to use an ionospheric correction model, the coefficients of which are transmitted as part of the GPS satellite message [Klobuchar, 1987]. This Klobuchar model is described by eight coefficients (four  $\alpha_i$ 's and four  $\beta_i$ 's) and removes about 50% of the ionospheric delay at mid-latitude. The correction is:

$$\delta P_{\text{ion}} = \begin{cases} F \cdot [DC + A \cos(2\pi(t - \Phi) / P)] & \text{day} \\ F \cdot DC & \text{night} \end{cases} \quad (5.10)$$

with

F slant factor

DC constant night-day offset (5 ns)

A amplitude

$\Phi$  constant phase offset ( 50400 seconds)

t local time

P period

and

$$A = \sum_{n=0}^3 \alpha_n \Phi^n \quad (\text{seconds}); \quad B = \sum_{n=0}^3 \beta_n \Phi^n \quad (\text{seconds});$$

An alternative method to model the ionosphere is to calculate the relative ionospheric effect through the combination of code and phase measurements, if

the code measurements are accurate enough. The GPS code and phase measurement equations on L1 can be written as:

$$p_{L1} = \rho + d\rho + c(dt - dT) + dp_{ion}^{L1} + d_{trop} + \varepsilon(p_{L1}) \quad (5.11)$$

$$\Phi_{L1} = \rho + d\rho + c(dt - dT) + d\Phi_{ion}^{L1} + d_{trop} + \lambda_1 N_{L1} + \varepsilon(\Phi_{L1}) \quad (5.12)$$

From equations (5.11) and (5.12), we find that the difference between code and phase measurements is related to the ionospheric effect as follows:

$$p_{L1} - \Phi_{L1} = dp_{ion}^{L1} - d\Phi_{ion}^{L1} - \lambda_1 N_{L1} + \varepsilon(p_{L1} - \Phi_{L1}) \quad (5.13)$$

The carrier phase multipath and measurement errors  $\varepsilon(\Phi_{L1})$  are two orders of magnitude smaller than the code multipath and measurement errors  $\varepsilon(p_{L1})$ . If we assume that the antenna site is in a low multipath environment, the averaged code measurement error  $\varepsilon(p_{L1})$  will be significantly smaller than the ionospheric effect. Thus,

$$p_{L1} - \Phi_{L1} \cong dp_{ion}^{L1} - d\Phi_{ion}^{L1} - \lambda_1 N_{L1} \quad (5.14)$$

or

$$dp_{ion}^{L1} = \frac{1}{2}(p_{L1} - \Phi_{L1} + \lambda_1 N_{L1}) \quad (5.15)$$

Since  $dp_{ion}^{L1}$  and  $d\Phi_{ion}^{L1}$  are equal but of opposite signs, the difference (or divergence) between the code and carrier measurements is twice the group delay plus a constant ambiguity. The key problem in estimating the absolute ionospheric effect with single frequency GPS measurements is to separate the cycle ambiguity from the ionospheric delay.

### 5.3.2 Separation of Carrier Phase Ambiguity and Ionospheric Delay

In order to separate the cycle ambiguity from the ionospheric delay, an obliquity function is introduced to map the vertical delay at the ionospheric intercept point to the line-of-sight delay at the user location [Cohen et al 1992]. The obliquity function  $O(E)$  can be expressed in terms of the satellite elevation angle,  $E$  [Klobuchar, 1987]:

$$O(E) = \sec[\sin^{-1}(0.94792 \cos E)] \quad (5.16)$$

which can be approximated numerically by:

$$O(E) = 1 + 2[(96 - E) / 90]^3 \quad (5.17)$$

From equation (5.15) we have:

$$p_{L1} - \Phi_{L1} = 2dp_v * O(E) - \lambda_1 N_1 \quad (5.18)$$

where  $dp_v$  is the vertical group delay at the ionospheric intercept point. Separating  $dp_v$  into a standard ionospheric correction  $I_S$  and a residual vertical delay  $dI_V$ , we obtain:

$$p_{L1} - \Phi_{L1} = 2(I_S + dI_V) * O(E) - \lambda_1 N_1 \quad (5.19)$$

or:

$$p_{L1} - \Phi_{L1} - 2I_S * O(E) = 2dI_V * O(E) - \lambda_1 N_{L1} \quad (5.20)$$

The standard ionospheric correction  $I_S$  can be set to zero or calculated using the broadcast ionospheric model [Klobuchar, 1987]. If  $I_S$  is set to zero, the initial or absolute part of the ionospheric delay is still modelled through the polynomial coefficients estimated with a batch least-squares method.

The residual vertical delay  $dI_V$  is a function of time, user location, satellite elevation and azimuth. If we assume that the vertical total electron content (TEC) remains constant in time over the observation period, the residual vertical delay can be approximately expressed as a function of the ionosphere intercept point position  $(\phi^*, \lambda^*)$ . Many functions can serve this purpose. First order spherical harmonic functions were used by Cohen et al. [1992] to model the residual vertical TEC. In this research, the following third order polynomial was found to produce satisfactory results:

$$\begin{aligned} dI_V = & a_{00} + a_{10}\phi^* + a_{11}\lambda^* + a_{20}\phi^{*2} + a_{21}\phi^*\lambda^* + a_{22}\lambda^{*2} \\ & + a_{30}\phi^{*3} + a_{31}\phi^{*2}\lambda^* + a_{32}\phi^*\lambda^{*2} + a_{33}\lambda^{*3} \end{aligned} \quad (5.21)$$

The ionospheric intercept point coordinates  $\phi^*$  and  $\lambda^*$  can be calculated as a function of the user location  $(\phi_0, \lambda_0)$ , and the satellite elevation,  $E$ , and azimuth,  $AZ$ :

$$\phi^* = \sin^{-1}(\sin \phi_0 \cos E + \cos \phi_0 \sin E \cos AZ) \quad (5.22)$$

$$\lambda^* = \lambda_0 + \sin^{-1}\left(\frac{\sin E \sin AZ}{\cos \phi^*}\right) \quad (5.23)$$

The 10 parameters  $a_{00}, a_{10}, a_{11}, a_{20}, a_{21}, a_{22}, a_{30}, a_{31}, a_{32}, a_{33}$ , along with the carrier phase cycle ambiguity  $N_{L1}$ , are estimated using a least-squares adjustment using the observables  $(p_{L1} - \Phi_{L1})$  over the observation period. The absolute group delay, in addition to its variation along the satellite trajectory during the observation period, can therefore be recovered.

### 5.3.3 Results and Analysis

Three sets of data are used herein to illustrate the code-carrier phase divergence concept using the formulation presented in the previous section. The first data set consists of dual frequency P code and carrier phase data collected with a Rogue receiver at a fixed site in Western Canada. The ionospheric effect estimated with the divergence technique using L1 data can be compared with the effect measured directly using dual-frequency measurements. The second data set includes data collected simultaneously with a dual-frequency Ashtech P-XII receiver and a narrow correlation spacing L1 C/A code NovAtel GPSCard™. The receivers were operating side by side in the Calgary area. The dual frequency P-code data can be compared to the divergence results obtained with the C/A code receiver. The third data set consists of GPSCard™ collected in the eastern USA in December, 1992 [Lachapelle et al., 1993] The ionospheric effect estimated with the divergence method is compared to the broadcast ionospheric model.

#### 1. P L1 Divergence Versus L1/L2 Ionospheric Results

Data collected by Geodetic Survey of Canada with a Rogue SNR-8C receiver at Station Albert Head, British Columbia, on April 27, 1993, over a four hour period was used. This station is part of the Canadian Active Control System (ACS). The P code observation noise, which includes receiver noise and field multipath, is estimated to be of the order of 10 - 20 cm for such a fixed site. The local time of the initial epoch was about 21:00. P-code and carrier phase measurements collected on L1 every 30 seconds were used to derive the code/carrier divergence. The broadcast ionospheric model was not recorded and the term  $I_5$  in equation (5.20) was set to zero. The 10 polynomial coefficients of

equation (5.21), together with  $N_{L1}$  in equation (5.20), were solved simultaneously with a least-squares adjustment. The *a posteriori* standard deviation of  $N_{L1}$  was of the order of 0.5 - 1.0 cycle.

The ionospheric effect derived with the divergence method is compared to that obtained using L1/L2 carrier phase measurements for the five satellites used in Figure 5.2. For each satellite, the L1 ionospheric group delay (or carrier phase advance if the sign is changed) obtained with the direct divergence measurements, i.e.,  $P(L1)-\Phi(L1)$ , its polynomial approximation, and the dual-frequency measurements, i.e.,  $\Phi(L1)-\Phi(L2)$ , are shown. The three sets of results are in very close agreement and can hardly be distinguished from one another. In the case of the dual-frequency measurements, the initial ionospheric delay, which would normally be set to zero due to the presence of the unknown carrier ambiguities  $N_{L1}$  and  $N_{L2}$ , was shifted to coincide with the initial delay estimated with the divergence technique. In order to obtain a qualitative estimate of the accuracy of the initial delay obtained with the divergence method, the numerical values of the initial delay obtained both with the divergence method and the dual-frequency P-code measurements at that epoch are given for each satellite. The L1/L2 initial delay is obtained with the following standard formula:

$$dp_{ion}^{L1}(L1/L2) = 1.5457[p(L1) - p(L2)] \quad (5.24)$$

The accuracy of the L1/L2 initial delay is estimated to be of the order of 25 - 50 cm. The results shown in Figure 5.2 show that the relative fit between the direct divergence measurements, the polynomial approximation and the dual-frequency measurements is very good, the rms difference between any two sets of results being better than 5 cm. This is due to the low code multipath

environment at the station and to relatively constant (in time) ionospheric conditions during the observation period. The differences in the initial delay range from 20 to 200 cm which is considered satisfactory, in view of the assumptions made to recover the initial delay with the divergence method and the possible difference of up to several nanoseconds between the satellite L1 and L2 code phase offsets [Cohen et al 1992]. Similar results were also achieved at other ACS stations and different observation periods.

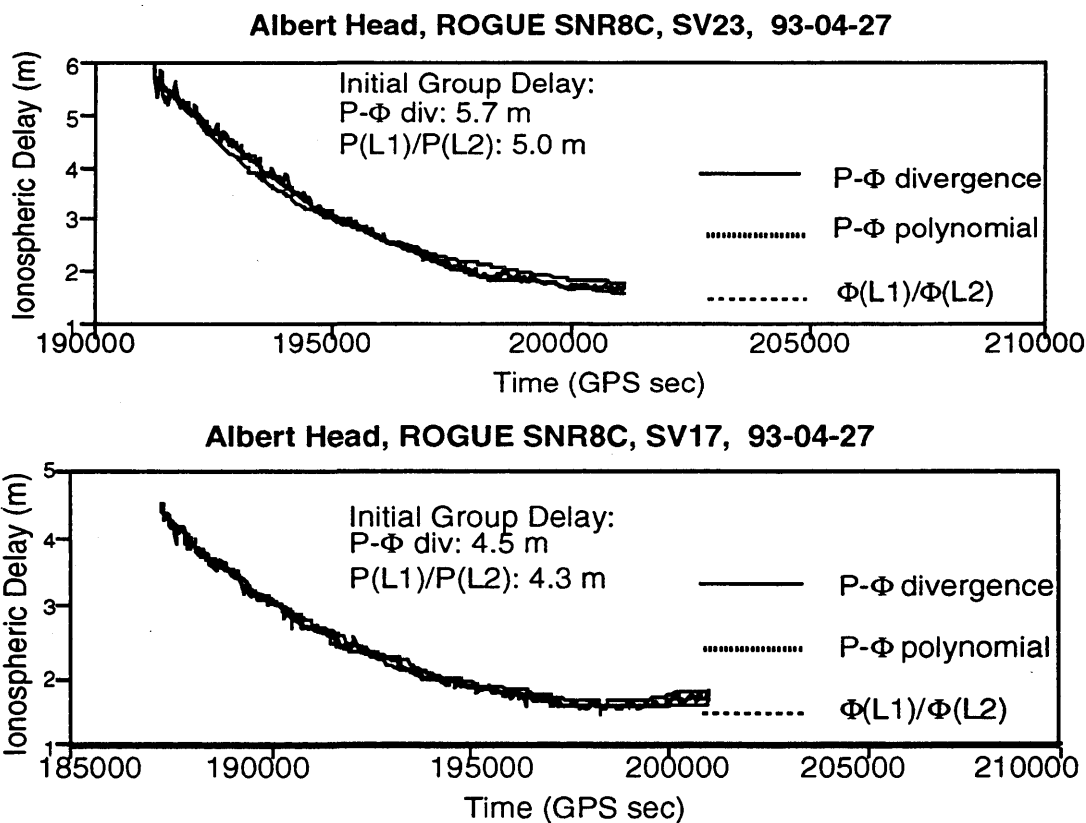


**Figure 5.2 (a): Comparison of Ionospheric Delay Estimated by the Dual-Frequency and P(L1) Code-Carrier Phase Divergence Methods (SV23 and SV17)**

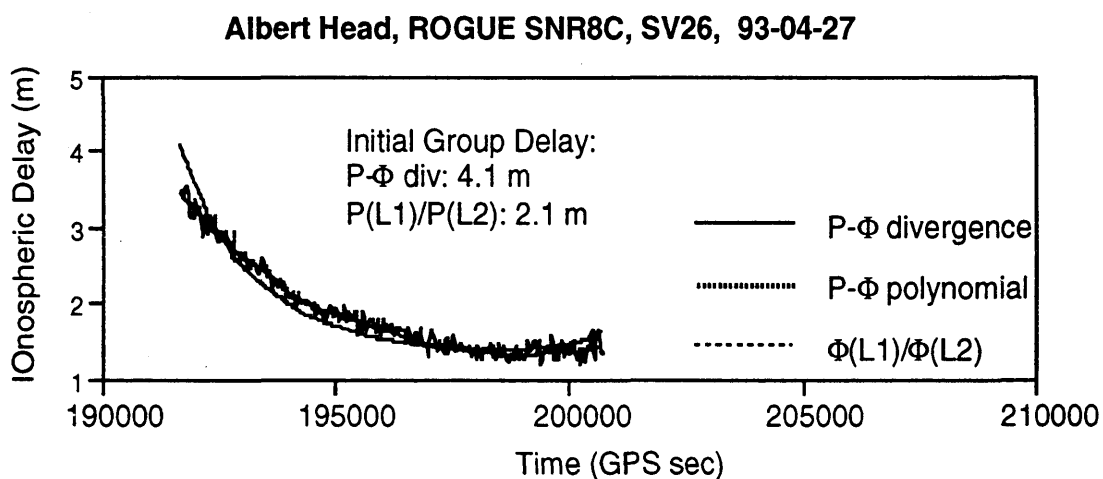
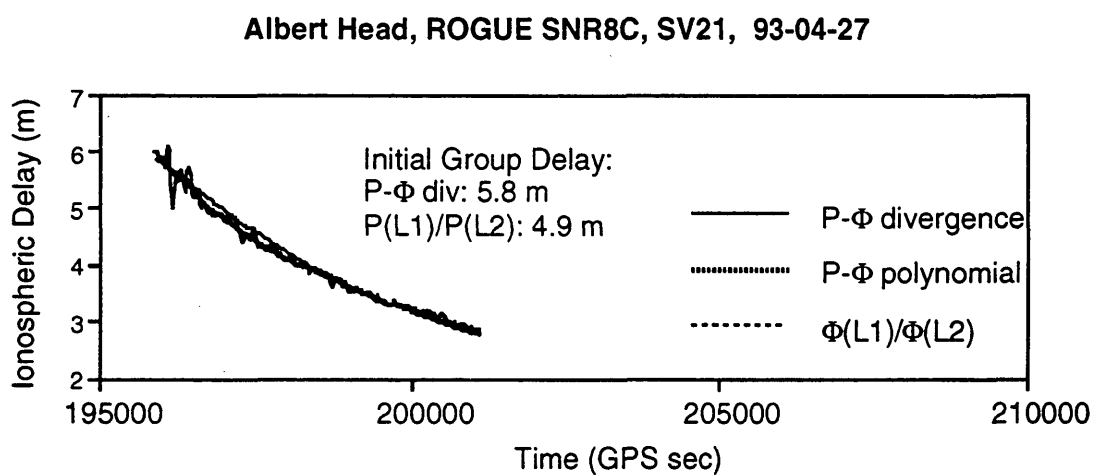
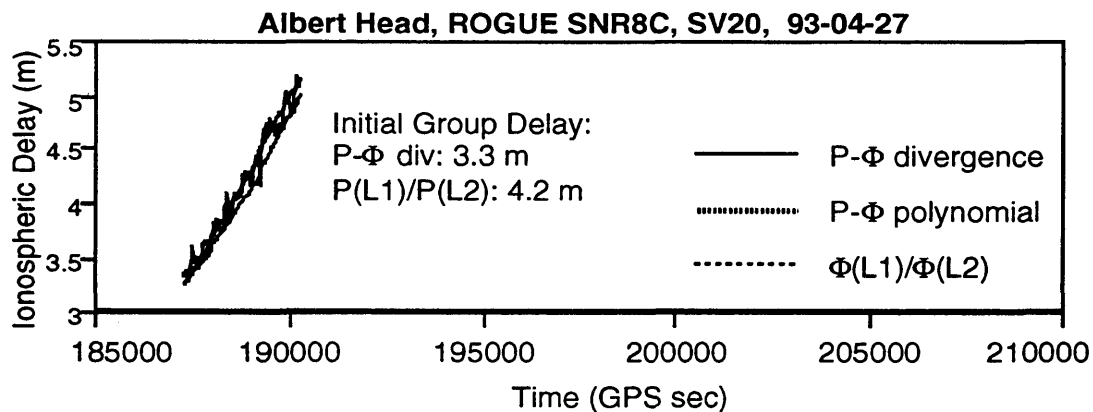


**Figure 5.2 (b): Comparison of Ionospheric Delay Estimated by the Dual-Frequency and P(L1) Code-Carrier Phase Divergence Methods (SV20, SV21, and SV26)**

## 2. C/A (L1) Divergence Versus L1/L2 Ionospheric Results

Data collected simultaneously with a dual-frequency Ashtech P-XII unit and a narrow correlation spacing L1 C/A code NovAtel GPSCard™ in August 1992 on the Springbank calibration baseline, located some 20 km West of Calgary, was used in this case. The two receivers were approximately 500 metres apart. Since significant code multipath was present, as is nearly always the case under normal field conditions, chokering ground planes were used with both receivers. Such ground planes were proven to be effective with both types of receivers to decrease multipath (e.g., Cannon & Lachapelle 1992a, b). As in the previous example,  $I_5$  was set to zero. The ionospheric effect derived with the GPSCard™ L1 divergence method is compared to that obtained using P-XII L1/L2 carrier phase measurements in Figure 5.3. The differences in the initial delay estimated using the divergence method and calculated using dual-frequency data range from 40 to 160 cm which is of the same order of magnitude as in the previous example.

Although the relative agreement is not as good as that shown in the previous example, the estimated ionospheric effect using the divergence method still agrees within 10 cm with that derived with the dual-frequency method. The differences are due to two reasons, namely the model assumption that the ionospheric effect remains constant during the observation period, and code multipath. This is illustrated in Figure 5.4 where a limited segment of divergence measurements  $[P_{C/A(L1)} - \Phi_{L1}]$  is shown for SV03 and SV21. Local irregularities are caused by a combination of the above phenomena.

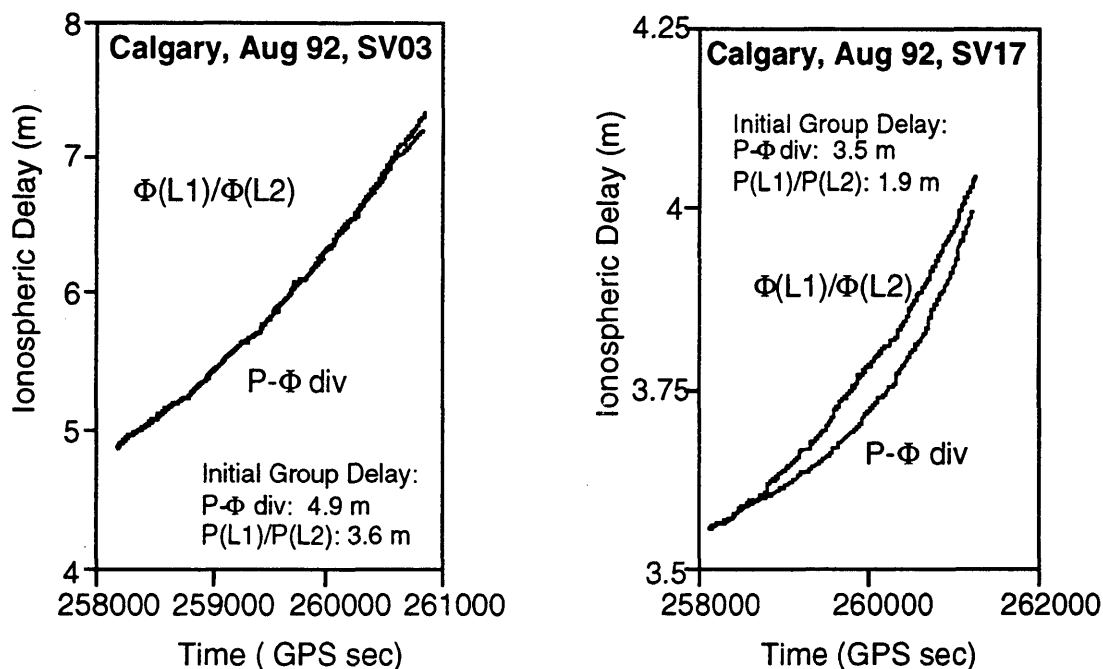


**Figure 5.3(a) Comparison of Ionospheric Delay Estimated by the Dual Frequency and C/A (L1) Code-Carrier Phase Divergence Methods (SV03 & SV17)**

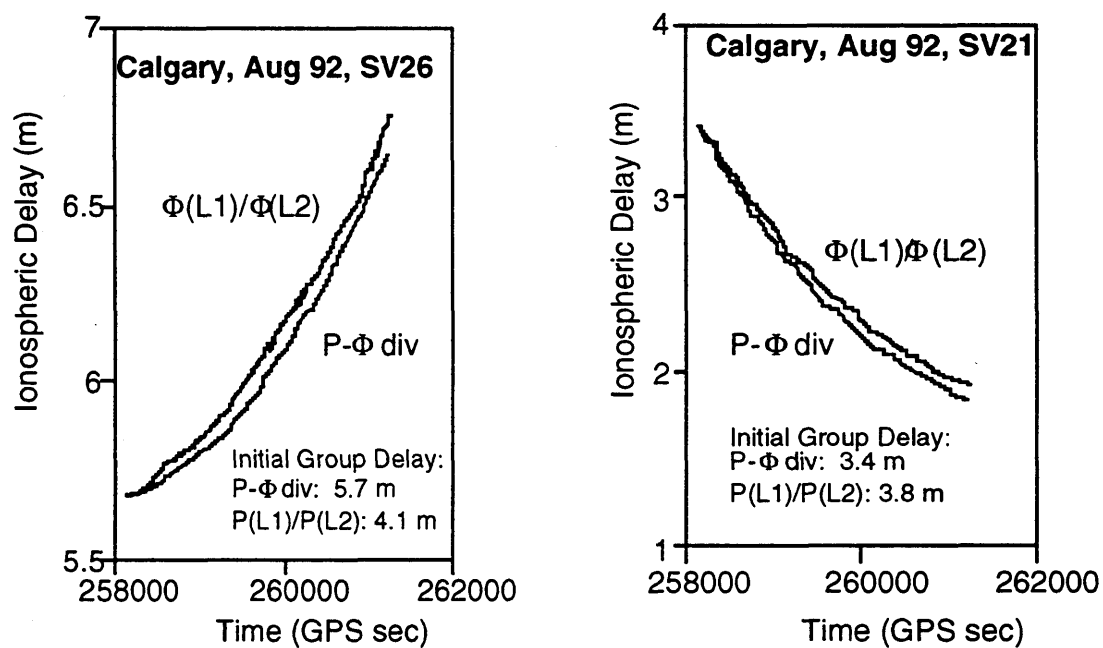


**Figure 5.3(b) Comparison of Ionospheric Delay Estimated by the Dual Frequency and C/A (L1) Code-Carrier Phase Divergence Methods (SV21 & SV26)**

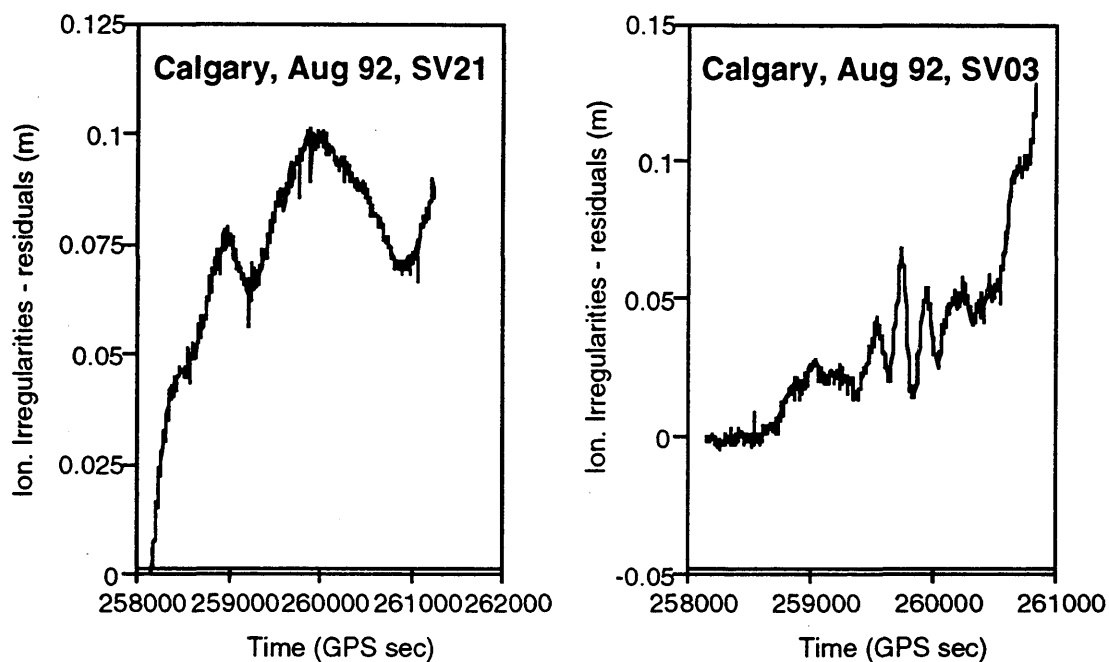


**Figure 5.4 Local Irregularities of Code-Carrier  
Phase Divergence Measurements**

**Table 5.4: Relative Error of the Ionospheric Delay Estimated  
with an L1 Narrow Correlator Spacing Receiver**

Satellite	$\max(\Delta dp_{\text{ion}})$	$\max(dp_{\text{ion}})$	Relative Error
SV03	0.13 m	2.40 m	5%
SV17	0.04	0.48	8%
SV21	0.09	1.49	6%
SV26	0.10	1.07	9%

As an accuracy indicator, the relative error of the ionospheric effect estimated using the GPSCard<sup>TM</sup> is shown in Table 5.4. The relative error (R.E.) is defined as:

$$\text{R.E.} = \max(\Delta dp_{\text{ion}}) / \max(dp_{\text{ion}}) \quad (5.25)$$

where  $\max(\Delta dp_{\text{ion}})$  is the maximum difference in the ionospheric effect calculated by the two receivers, and  $\max(dp_{\text{ion}})$  is the maximum variation of the ionospheric effect during the observation period. The relative error reaches

9% which means that the L1 code and carrier phase divergence method can remove 90% of the relative ionospheric effect.

### 3. C/A (L1) Divergence Versus Broadcast Ionospheric Model

A data set collected on December 8, 1992, in Virginia with a NovAtel GPSCard™ [Lachapelle et al., 1993] was chosen to compare the ionosphere delay estimated by code/carrier phase divergence with that derived using the broadcast ionospheric model. No dual frequency measurements were available. The measurements were made between 10:00 and 13:00, local time. During a 3-hour observation period, seven satellites were tracked. The trajectories of three selected satellites are shown in Figure 5.5. A data interval of 10 seconds was used to obtain the divergence results. In this case,  $I_S$  values calculated from the broadcast model were used.

Shown in Figure 5.6 and 5.7 for the three selected satellites are the code-carrier phase divergence measurements, the corresponding polynomial models, and the broadcast ionospheric models. The relative ionospheric effect estimated by the divergence method is in a good agreement with the broadcast model. The differences between the initial delays obtained with the two methods range between 20 cm in the case of SV12 to 3.02 m in the case of SV23. The broadcast model has an estimated accuracy of 50% at mid-latitude and the differences are therefore well within the error range. Another set of polynomial models was derived using  $I_S$  values of 0. The only differences were in the initial ionospheric delays. These range from -1.8 m to 3.7 m. Again, this is well within the above range of uncertainty. Additional tests with the availability of a dual-frequency

receiver to measure directly the absolute ionospheric delay are however required to better assess the effectiveness of the above approaches.

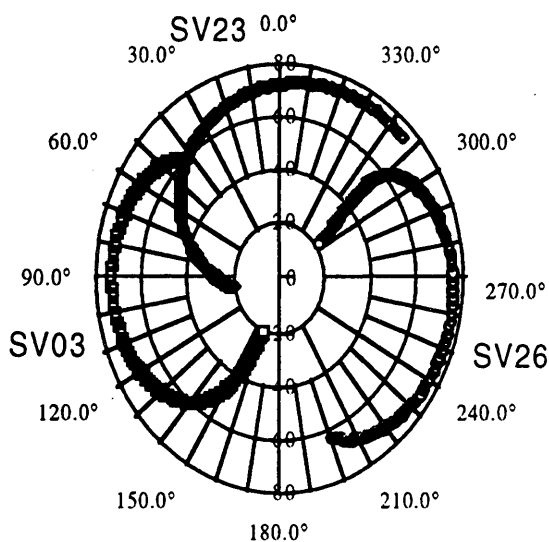


**Figure 5.5 Polar Plots of Satellites, 10:00 - 13:00, December 8, 1992**

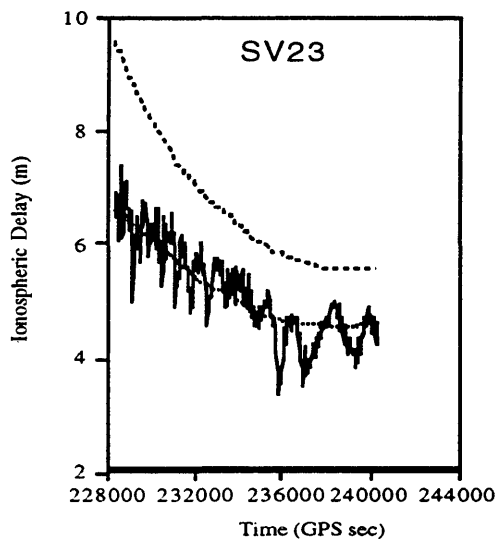


**Figure 5.6 Broadcast Ionospheric Delay Versus Delay Estimated using Code/Carrier Divergence (SV23)**

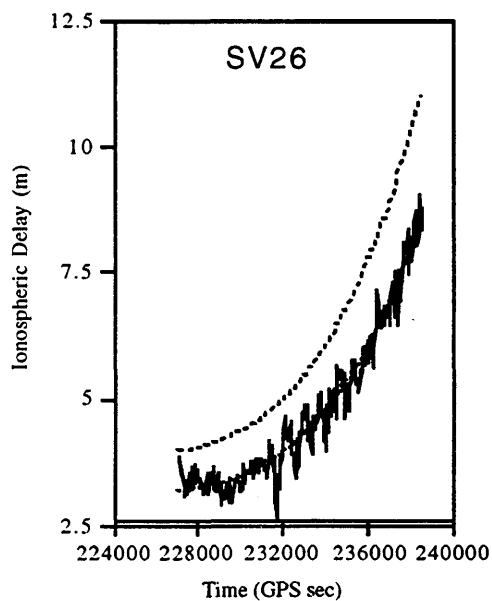
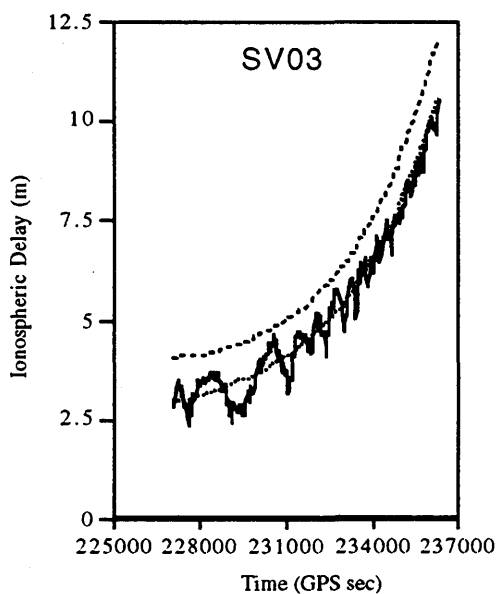


**Figure 5.7 Broadcast Ionospheric Delay Versus Delay Estimated Using The Code/Carrier Phase Divergence Method (SV03 and SV26)**

### 5.3.4 Recovery of the Ionospheric Delay with the Divergence Method for Baseline Determination

The performance of the code-carrier phase divergence method to recover the relative effect of the ionosphere for precise baseline determination were investigated. Since double differenced carrier phase observations are normally used in such a case, only the relative ionospheric effect with respect to the initial observation epoch is required and the initial ionospheric delay is not needed. In principle, direct code-carrier phase divergence measurements (e.g.,  $p_{L1} - \Phi_{L1}$ ) could therefore be used. However, the polynomial model presented earlier is still useful as it acts as a filter to reduce the effects of code multipath.

Three baselines of the Canadian Active Control System located in British Columbia were used. These are shown in Figure 5.8. The baseline lengths vary between 302 and 627 km and their heights between 32 and 560 m. The baseline coordinates are known with an accuracy better than a few cm from previous VLBI and GPS surveys. One of the stations, namely Albert Head (ALBH), was used to assess the effectiveness of the divergence method in single point mode in the previous section. All three stations were observed with dual-frequency Rogue SNR-8C receivers. The baselines could therefore be processed using successively L1 only, L1/L2 and L1 data corrected for the effect of the ionosphere using the code/carrier phase divergence method. Data over three different days, namely, Julian Day 116, 117 and 144, were processed to assess the repeatability of the results. Some three to four hours of data per day, at an interval of 30 seconds, was used.

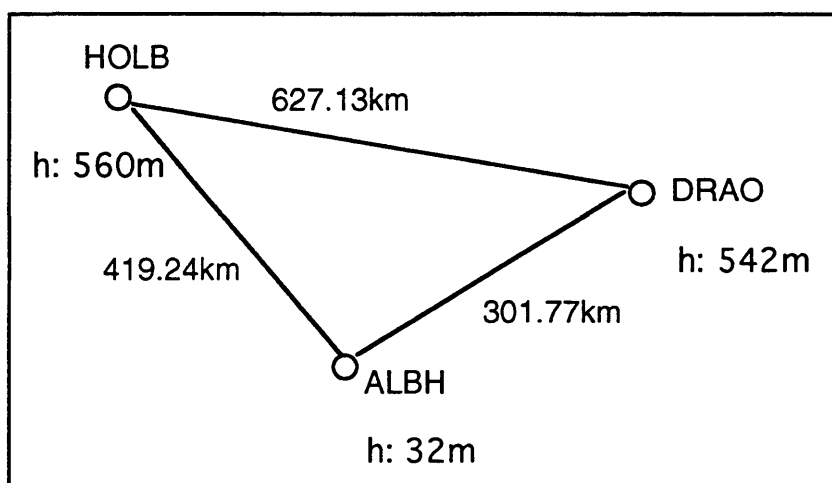


**Figure 5.8 ACS Stations Used for Baseline Test**

Because of the use of external frequency standards at ACS stations and double differencing, the effect of receiver and satellite clock errors on baseline solutions were eliminated. In order to remove the effect of broadcast ephemeris errors, precise post-mission orbits calculated by the Geodetic Survey of Canada were used. These have an estimated accuracy of 1 m. The raw L1 and ionospherically corrected L1 carrier phase data was post-processed in double difference mode, with real number ambiguities estimated as part of the solution. The remaining errors present in the L1/L2 solutions, therefore, consist mostly of tropospheric errors. The L1 solution is affected by the same tropospheric errors and by ionospheric errors. The difference between the L1 and L1/L2 solutions is therefore due to the ionospheric effect. The L1 solutions corrected for the effect of the ionosphere with the divergence method are also affected by the same tropospheric errors. Differences between these solutions and the L1/L2 solutions are caused by the limitations of the divergence method to account for the entire ionospheric effect.

**Table 5.5 Comparison of L1, L1/L2 and Code/Carrier Divergence Solutions  
(Baseline ALBH-DRAO, 301.77km)**

Date	Obs	$\Delta\phi$ (m)	$\Delta\lambda$ (m)	$\Delta h$ (m)
	L1	0.001	0.030	-0.158
Day116	L1/L2	-0.006	0.033	-0.033
	CCD*	0.035	-0.015	-0.079
	L1	-0.017	0.678	0.028
Day117	L1/L2	-0.011	0.028	-0.057
	CCD	0.051	0.113	-0.174
	L1	0.243	0.369	-0.069
Day144	L1/L2	-0.009	0.025	0.051
	CCD	0.087	0.094	0.076

\* CCD: Ionospheric effect calculated by code/carrier divergence.

**Table 5.6 Comparison of L1, L1/L2 and Code/Carrier Divergence Solutions  
(Baseline ALBH-HOLB, 419.24km)**

Date	Obs	$\Delta\phi$ (m)	$\Delta\lambda$ (m)	$\Delta h$ (m)
	L1	-0.457	0.124	0.331
Day116	L1/L2	0.043	0.017	-0.083
	CCD	-0.030	0.113	0.033
	L1	-0.032	-0.556	-0.245
Day117	L1/L2	0.031	0.000	-0.042
	CCD	0.037	0.103	-0.154
	L1	-0.218	-0.221	0.130
Day144	L1/L2	0.028	0.020	-0.052
	CCD	0.050	0.089	0.029

**Table 5.7 Comparison of L1, L1/L2 and Code/Carrier Divergence Solutions  
(Baseline DRAO-HOLB, 627.13km)**

Date	Obs	$\Delta\phi$ (m)	$\Delta\lambda$ (m)	$\Delta h$ (m)
	L1	-0.240	-0.085	-0.119
Day116	L1/L2	0.038	-0.037	-0.009
	CCD	0.020	-0.160	-0.050
	L1	0.062	-0.233	-0.471
Day117	L1/L2	0.045	-0.045	-0.010
	CCD	0.027	0.064	0.019
	L1	0.107	-0.210	-0.299
Day144	L1/L2	0.029	-0.027	-0.116
	CCD	0.013	0.031	-0.153

**Table 5.8 RMS Fit of L1, L1/L2 and Code/Carrier Divergence Solutions**

Solution	Latitude	Longitude	Height	3D RSS*
L1	21 cm	6 cm	24 cm	48 cm
L1/L2	3	3	6	7
CCD	4	10	10	15

\* Root Sum Square

Differences in latitude, longitude and height components between the known values and the solutions described above are given in Table 5.5, 5.6, and 5.7. The L1/L2 differences are largest in the height component and reach 12 cm for the baseline DRAO-HOLD on Day 144. These differences are likely due to residual tropospheric effects. The L1 differences reach 68 cm in longitude for the baseline

ALBH-DRAO on Day 117. The CCD L1 differences reach 17 cm in height for the baseline ALBH-DRAO on Day 117. More statistically significant than the above differences, however, are the rms and difference statistics given in Table 5.8. The accuracy gain from an L1 only to an L1/L2 solution is evident with a three-dimensional root sum square (RSS) decrease of 48 to 7 cm. The use of CCD L1 solutions result in an RSS of 15 cm, a significant improvement over the L1-only RSS fit.

The proposed approach of recovering ionospheric effect using a single frequency code/carrier phase divergence was also successfully applied to the long baseline data reduction of a series of surveys conducted in Eastern United States in December 1992 with GPSCard™. The use of this method was shown to produce significantly better results over L1 only carrier phase solution, thereby demonstrating the capability of narrow correlator spacing single frequency equipment for ionospheric effect recovery [Cannon et al., 1994].

## CHAPTER 6

### CONCLUSIONS AND RECOMMENDATIONS

In this thesis, ambiguity search strategies for rapid static surveying are discussed and some modifications are explored. Based on the assumption that the impact of the periodic multipath error on code and carrier phase measurements can be minimized by averaging the observations, an attempt is made to estimate the site occupation time in order to correctly resolve the integer ambiguities. For single frequency users, an ionospheric model is developed by using code and carrier phase measurements. The accuracy of this model and results of baselines by applying this model are analysed.

Based on the investigations done in this research and the results obtained from the data processing, the following conclusions can be made.

The ambiguity resolution prediction algorithm can be employed in real-time to inform the user when sufficient measurements have been taken to resolve the ambiguities in rapid static surveys. The algorithm is simple and self-contained. Under favorable conditions (low multipath environment), the success rate of this predictor is very high. However, the usage of such a predictor without using any actual measurements has some severe limitations. One has to assume that every available satellite can actually be tracked by all the receivers. The procedure relies on the assumption that the actual noise level in the measurements is very close to the a priori value used in the algorithm.

Carrier phase multipath will strongly degrade the data quality and thus affect the site occupation time needed to resolve the ambiguities. Multipath errors in pseudorange measurements can be detected by analysing the differences between ionospherically corrected pseudorange and carrier phase observations. For short baselines, multipath errors in carrier phase measurements can be detected by analysing the differential ionospheric delay using dual-frequency data. Both chokering and RF absorbent planes are very effective in reducing multipath. In order to resolve the integer ambiguities with a high level of certainty in rapid static surveys, the site occupation periods should be as long as the largest multipath period, provided that the satellite geometry is optimal.

For short baselines, the ionospheric effect virtually cancels in double differencing mode. The application of the ionospheric correction to the raw data increases the measurement noise and multipath. However, as the baseline length increases, the accuracy of double difference carrier phase solutions without ionospheric correction will be degraded and finally lead to a level which might not be acceptable for certain GPS surveys.

The code-carrier phase divergence methodology used herein to recover the ionospheric group delay or carrier phase advance with single-frequency observations was shown to be effective for the cases analysed with P-code and narrow correlator spacing C/A receivers, with over 90% of the effect recovered. Many conditions are however required for the method to be applied successfully, namely, the absence of irrecoverable cycle slips from the observation sequence, a relatively low code multipath environment, and a relatively constant ionosphere during the observation period. The first condition can usually be met for most

differential static applications where cycle slip recovery can be achieved with a relatively high degree of success. The second condition can often be met through a combination of careful siting, antenna design, and the use of choking ground planes to reduce multipath sources. The latter condition could partly be overcome by using an appropriate analytical model. For some types of precise DGPS kinematic missions where the monitor-remote distance may necessitate the recovery of the absolute part of the ionospheric delay, the code-carrier divergence technique may find some use provided that the above conditions can be met.

The research reported in this thesis did not provide all the answers to the effects of critical error sources in static surveys, which in itself is a multi-faceted problem. Some aspects have not been investigated, such as tropospheric effect, orbital errors, Selective Availability (SA), and others need more investigations. The following investigations are recommended as a continuation of this research.

(1) One of the greatest challenges with rapid static surveying techniques is the judicious decision as to whether a solution is good enough to confirm that integer ambiguities have been successfully resolved. Applications of statistical criteria are complicated by the existence of systematic errors such as multipath. More investigations are required in this area.

(2) In this thesis, dual-frequency carrier phase measurements are used to detect carrier multipath errors. However, as the type of receiver used by the majority of civilian users will be of the less expensive, single frequency kind, other methods to detect carrier phase multipath should be used. New receiver

architectures and in-receiver signal processing techniques for GPS multipath reduction should also be investigated.

(3) The empirical relationship between site occupation time and major multipath periods presented in this thesis is based on limited GPS data sets. A wider variety of GPS data should be analysed in order to have more insight into the effect of multipath on the resolution of integer ambiguities.

(4) The ionospheric model developed in this thesis is based on the assumption that the Total Electron Content (TEC) remains constant within the observation period. With the use of more stations, more sophisticated models could be used to describe the variation of the ionospheric delay which, in turn, will improve the accuracy of the estimated absolute ionospheric delay.

(5) The relationship between code and carrier phase multipath demonstrated in this thesis should be further investigated to determine whether code measurements could be used in real-time to quantify the level of carrier phase multipath and estimate the observation time for successful ambiguity resolution.

## REFERENCES

- Abidin, H. (1990): "Extra-widelanding for 'On the Fly' Ambiguity Resolution: Simulation of Multipath Effects." ION GPS-90, Colorado Springs, CO.
- Abidin, H. Z. and D.E. Wells (1990): "Extra-Widelaning for 'On the Fly' Ambiguity Resolution: Simulation of Ionospheric Effects." Proceedings of the Second International Symposium on Precise Positioning with the Global Positioning System, The Canadian Institute of Surveying and Mapping.
- Abidin, H. Z. (1993): "Computational and Geometrical Aspects of On-the-Fly Ambiguity Resolution. Ph.D. Dissertation, Department of Surveying Engineering Technical Report No. 164, University of New Brunswick, Fredericton, New Brunswick, Canada.
- Bassiri, S and George A. Hajj (1993): "Higher-order Ionospheric Effects on the Global Positioning System Observables and Means of Modeling Them." *Manuscripta Geodaetica* Vol.18, No.5.
- Beutler, G., W. Gurtner, I. Bauersima, and R. Langley (1985): "Modeling and Estimating Orbits of GPS Satellites." Proceedings of the First Symposium on Precise Positioning with the Global Positioning System.

- Beutler, G., W. Gurtner, U. Hugentobler, M. Rothacher, T. Schildknecht, U. Wild (1988): "Ionosphere and GPS Processing Techniques." Chapman Conference on GPS Measurements for Geodynamics, Fort Lauderdale, Florida, USA.
- Bishop, G., J. Klobuchar and P. Doherty (1985): "Multipath Effects on the Determination of Absolution Ionospheric Time Delay From GPS Signals." *Radio Science*, Vol. 20., No. 3.
- Cannon, M. E. (1990): "High-accuracy GPS Semikinematic Positioning: Modeling and Results." *Navigation*, Journal of the Institute of Navigation, Vol. 37, No. 1.
- Cannon, M. E., G. Lachapelle, H. Ayers, K. P. Schwarz (1990): "A Comparison of SEMIKIN and KINSRVY for Kinematic Applications." Proceedings of ION GPS-90, Colorado Springs.
- Cannon, M. E. and G. Lachapelle (1992): "Analysis of A High Performance C/A Code Receiver in Kinematic Mode." ION National Technical Meeting, San Diego.
- Cannon, M. E., G. Lachapelle, W. Qiu, S. L. Frodge, and B. Remondi (1994): "Performance Analysis of A Narrow Correlator Spacing Receiver for Precise Static DGPS Positioning." Proceedings of IEEE PLANS-94, Las Vegas (in press).
- Chen, D.S. (1993): "Fast Ambiguity Search Filter (FASF): a Novel Concept for GPS Ambiguity Resolution." Proceedings of ION GPS-93, Salt Lake City, The Institute of Navigation, Washington, D.C..

- Cohen, C., B. Parkinson (1991): "Mitigating Multipath Error in GPS Based Attitude Determination." *Guidance and Control, Vol.74, Advances in the Astronautical Science.*
- Cohen, C., B. Pervan, B. Parkinson (1992): "Estimation of Absolute Ionospheric Delay Exclusively through Single-frequency GPS Measurements.", *Proceedings of ION GPS-92, Albuquerque, New Mexico.*
- Counselman, C. C. and S. A. Gourevitch (1981): "Miniature Interferometer Terminals for Earth Surveying: Ambiguity and Multipath with Global Positioning System." *IEEE Transactions on Geoscience and Remote Sensing, Vol. GE-19, No. 4.*
- Elgered, G., B. Rönnäng, E. Winberg, J. Askue (1985): "Satellite-Earth Measurements I. Correction of the Excess Path Length due to Atmospheric Water Vapour by Ground Based Microwave Radiometry. Research Report No. 147, Res. Lab. El. and Onsala Space Observatory Gothenberg, Sweden.
- Erickson, C. (1992): "Investigations of C/A Code and Carrier Measurements and Techniques for Rapid Static GPS Surveys." MSc Thesis, Publication No. 20044, Department of Geomatics Engineering, The University of Calgary.
- Evans, A. (1986): "Comparison of GPS Pseudorange and Biased Doppler Range Measurements to Demonstrate Signal Multipath Effects." *International Telemetry Conference, Las Vegas, NV.*
- Falkenberg, W. G., P. Kielland and G. Lachapelle (1988): "GPS Differential Positioning Technologies for Hydrographic Surveying." *Position, Location and Navigation Symposium (PLANS), Orland, FL.*

- Frei, E., and G. Beulter (1990): "Rapid Static Positioning Based on the Fast Ambiguity Resolution Approach 'FARA': Theory and First Results." *Manuscripta Geodaetica*, Vol. 15.
- Frei, E. (1991): "Rapid Static Differential Positioning with The Global Positioning System (GPS)." *Geodätischen-geophysikalische Arbeiten in der Schweiz*, Band 44.
- Fu, X. (1992): "Investigation of Multipath Carrier Phase Effects in GPS Hydrographic Applications." Proceedings of ION GPS-92, New Mexico.
- Gelb, A (1974): *Applied Optimal Estimation*. M.I.T Press, Cambridge Mass.
- Georgiadou, Y. and A. Kleusberg (1988a): "On Carrier Signal Multipath Effects in Relative GPS Positioning." *Manuscripta Geodaetica*, Vol. 13.
- Georgiadou, Y., and A. Kleusberg (1988b): "On The Effect of Ionospheric Delay on Geodetic Relative GPS Positioning." *Manuscripta Geodetica*, Vol. 13, No. 13.
- Graas, F. V., and Michael S. Braasch (1991): "Guidance Accuracy Consideration for Real-time GPS Interferometry." Proceedings of The GPS-91 Conference of The Satellite Division of The Institute of Navigation.
- Hagerman, L. L. (1973): "Effects of Multipath on Coherent and Noncoherent PRN Ranging Receiver." Aerospace Corporation Report No. TOR-0073(3020-03), 1973.

- Hatch, R. (1991a): "Instantaneous Ambiguity Resolution." Proceedings of IAG International Symposium 107 on Kinematic Systems in Geodesy, Surveying and Remote Sensing, Springer Verlag, New York.
- Hatch, R. (1991b): "Ambiguity Resolution while Moving - Experimental Results." Proceedings of ION GPS'91, Albuquerque, N. M., The Institute of Navigation, Washington, D.C.
- Hopfield, H. (1971): Tropospheric Effects on Electromagnetically Measured Range: Prediction from Surface Weather Data." *Radio Science* Vol.6 No. 3.
- Klobuchar, J. A. (1987): " Ionospheric Time-delay Algorithm for Single-frequency GPS users. *IEEE Transactions on Aerospace and Electronic Systems*, Vol. AES-23, No. 2.
- Krakiwsky, E. J. (1990): "The Method of Least Squares: A Synthesis of Advances." Lecture Notes 42, Department of Surveying Engineering, The University of New Brunswick (1975). Reprinted as Pub. 10003 of the Department of Surveying Engineering, The University of Calgary.
- Lachapelle, G., W. Falkenberg, D. Neufeldt and P. K. Keilland (1989): "Marine DGPS Using Code and Carrier in a Multipath Environment." ION GPS-89, Colorado Springs, CO.
- Lachapelle, G., M. E. Cannon, G. Lu (1992a): "High-Precision GPS Navigation with Emphasis on Carrier-Phase Ambiguity Resolution.", *Marine Geodesy* Vol. 15.

- Lachapelle, G., P. Kielland, and M. Casey (1992b): "GPS for Marine Navigation and Hydrography." *International Hydrographic Review*, Monaco, Vol. LXIX, No. 1.
- Lachapelle, G., M. E. Cannon, and G. Lu (1992c): "Ambiguity Resolution On-the-fly - A Comparison of P Code and High Performance C/A Code Receiver Technologies." *Proceedings of GPS-92*, Institute of Navigation, Alexandria.
- Lachapelle (1992d) *GPS: Theory and Applications*. ENSU 625 Lecture Notes, Department of Geomatics Engineering, The University of Calgary.
- Lachapelle, G., M. E. Cannon, C. Erickson, and W. Falkenberg (1992e): "High Precision C/A Code Technology for Rapid Static DGPS Surveys. SPN - Journal for Satellite Based Positioning, Navigation and Communication, Herbert Wichmann Verlag, Karlsruhe.
- Lachapelle, G., M. E. Cannon, B. Townsend, and W. Qiu (1993): "Investigation of the Accuracy of The DGPS Method Using the NovAtel GPSCard™." Contract Report submitted to Battelle Research Triangle Park Office for U.S. Army Topographic Engineer Centre, Fort Belvoir, VA.
- Landau, H. and H. J. Euler (1992): "On-the-Fly Ambiguity Resolution for Precise Differential Positioning." *Proceedings of IO GPS-92*, Albuquerque, New Mexico.
- Langley, R. B. (1992): "The Effect of The Ionosphere and Troposphere on Satellite Positioning Systems." Paper presented at the Symposium on Refraction of Transatmospheric Signals in Geodesy, The Hague, Netherlands.

- Leick, A. (1990) *GPS Satellite Surveying*, John Wiley, New York, NY.
- Lichten, S. M. and W. I. Bertiger (1989): "Demonstration of Sub-meter GPS Orbit Determination and 1.5 Parts in  $10^8$  Three-Dimensional Baseline Accuracy." *Bulletin Geodesique*, Vol. 63.
- McNamara, L.F. and P.J. Wilkinson (1983): "Prediction of Total Electron Content Using International Reference Ionosphere." *Journal of Atmospheric and Terrestrial Physics*, Vol. 45, No. 2/3.
- Meehan, T., and L.E. Yong (1992): "On Receiver Signal Processing for GPS Multipath." Proceedings of ION GPS-92, New Mexico.
- Merminod, B. (1988): "The Resolution of the Cycle Ambiguities." Report to the Swiss Science Foundation, University of New South Wales.
- Qiu, W., G. Lachapelle, M. E. Cannon (1993): "Ionospheric Effect Modeling for Single Frequency GPS Users." Submitted to *Manuscripta Geodaetica*, Springer Verlag, September. (Ref # PAC/13).
- Remondi, B. (1984): "Using the Global Positioning System (GPS) Phase Observable for Relative Geodesy: Modeling, Processing, and Results." Ph.D. Dissertation, Center for Space Research, The University of Texas at Austin, Austin.
- Rocken, C., and C. Meertens (1991): "Monitoring Selective Availability Dither Frequencies and Their Effect on GPS Data." *Bulletin Geodesique*, Vol. 65.
- Seeber, G (1993): *Satellite Geodesy*, Walter de Gruyter, Berlin, New York.

- Talbot, N. (1991): "Sequential Phase Ambiguity Resolution for Real-Time Static Differential GPS Positioning." *Manuscripta Geodaetica*, Vol. 16.
- Van Dierendonck, A. J., P. Fenton, and T. Ford (1992): "Theory and Performance of Narrow Correlator Spacing in A GPS Receiver." ION National Technical Meeting, San Diego.
- Vanicek, P., G. Beutler, A. Kleusberg, R.B. Langley, R. Santerre, D. E. Wells (1985): "DIPOP: Differential Positioning Program Package for the Global Positioning System." Geodetic Survey of Canada, Report No. 85-005, Ottawa.
- Wells, D. E., N. Beck, D. Delikaraoglou, A. Kleusberg, E. J. Krakiwsky, G. Lachapelle, R. B. Langley, M. Nakiboglu, K. P. Schwarz, J. M. Tranquilla, P. Vanicek (1987): *Guide to GPS Positioning*, Canadian GPS Associates, Fredericton, N. B.
- Wells, D. E., W. Lindlohr, B. Schaffrin, E. Grafarend (1987): "GPS Design: Undifferenced Carrier Beat Phase Observations and the Fundamental Differencing Theorem." Technical Report No. 116, Department of Surveying Engineering, University of New Brunswick, Fredericton, N. B.
- Wooden, W. H. (1985): "Navstar Global Positioning System: 1985." Proceedings of the First International Symposium on Precise Positioning with the Global Positioning System, Rockville, Maryland.
- Wübbena, G. (1989): "The GPS Adjustment Software Package-GEONAP - Concepts and Models." Proceedings of the 5th International Geodetic

Symposium on satellite Positioning, New Mexico State University, Las Cruces, N.M., Vol. 1.

Xia, R. (1992): "Determination of Absolute Ionospheric Error Using a Single Frequency GPS Receiver.", Proceedings of ION GPS-92, Albuquerque, New Mexico.